



저작자표시-비영리-변경금지 2.0 대한민국

이용자는 아래의 조건을 따르는 경우에 한하여 자유롭게

- 이 저작물을 복제, 배포, 전송, 전시, 공연 및 방송할 수 있습니다.

다음과 같은 조건을 따라야 합니다:



저작자표시. 귀하는 원저작자를 표시하여야 합니다.



비영리. 귀하는 이 저작물을 영리 목적으로 이용할 수 없습니다.



변경금지. 귀하는 이 저작물을 개작, 변형 또는 가공할 수 없습니다.

- 귀하는, 이 저작물의 재이용이나 배포의 경우, 이 저작물에 적용된 이용허락조건을 명확하게 나타내어야 합니다.
- 저작권자로부터 별도의 허가를 받으면 이러한 조건들은 적용되지 않습니다.

저작권법에 따른 이용자의 권리는 위의 내용에 의하여 영향을 받지 않습니다.

이것은 [이용허락규약\(Legal Code\)](#)을 이해하기 쉽게 요약한 것입니다.

[Disclaimer](#)

Customized Energy Down-Shift using Iridium Complexes for Enhanced Performance of Polymer Solar Cells

Jeong Hyuk Ahn

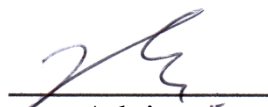
Department of Chemistry
Graduate School of UNIST

Customized Energy Down-Shift using Iridium Complexes for Enhanced Performance of Polymer Solar Cells

A thesis
submitted to the Graduate School of UNIST
in partial fulfillment of the
requirements for the degree of
Master of Science

Jeong Hyuk Ahn

06. 07. 2016
Approved by



Advisor
Tae-Hyuk Kwon

Customized Energy Down-Shift using Iridium Complexes for Enhanced Performance of Polymer Solar Cells

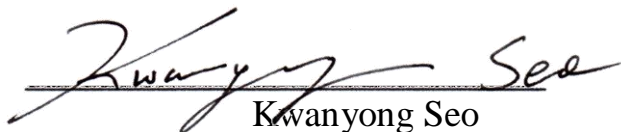
Jeong Hyuk Ahn

This certifies that the thesis of Jeong Hyuk Ahn is approved.

06. 07. 2016



Advisor: Tae-Hyuk Kwon



Kwanyong Seo



Jongnam Park

Abstract

For the higher performance of polymer solar cells (PSCs), many researchers tried to develop new polymers that can absorb broader range of spectrum. However, there are some limits to absorb broader range with single donor. Therefore, multi donor systems and energy transfer systems have been researched. With two different donors it is easier to enhance absorption range. As a result, multi donor and energy transfer was successful to increase performance. However, the existing systems are applying polymer-polymer systems. When two different polymers are mixed, the compatibility between two polymers is critical to morphology of blend film. Also, in polymer-polymer energy transfer, the boundary between charge transfer and energy transfer is unclear. Therefore, for the first time, we developed customized iridium (Ir(III)) complexes, with Ir(III) complex incorporated into the active materials poly(thieno[3,4-b]-thiophene/benzodithiophene) (PTB7, amorphous) or poly(3-hexylthiophene) (P3HT, high crystalline) as energy donor additives. The Ir(III) complex with the 2-phenyl quinolone ligand energy donor increased the power conversion efficiency of the corresponding devices by approximately 20%. The enhancements are attributed to the improved molecular compatibility and energy level between the Ir(III) complex and the active materials, long Förster resonance energy transfer radius, and high energy down-shift efficiency. Overall, we reveal Ir(III) complex additives for amorphous and highly crystalline polymer active materials; these additives would enable efficient energy transfer in polymer solar cells, while retaining the desirable active layer morphology, thereby resulting in improved light absorption and conversion.

Contents

I. Introduction	1
1.1 Polymer solar cells (PSCs)	1
1.1.1 Development of PSCs	1
1.1.2 Structure and mechanism of PSCs	2
1.1.3 Characterization of PSCs	4
1.2 Trends of research in PSCs	4
1.2.1 Single donor system	4
1.2.2 Multi donor system	6
1.2.3 Energy transfer system	8
1.3 Energy transfer	9
1.3.1 Mechanism	9
1.3.2 Conditions for efficient energy transfer	10
1.4 Iridium complexes	10
II. Results and Discussion	13
2.1 Synthesis of iridium (Ir(III)) complexes.....	13
2.2 Photophysical and electrochemical studies of Ir(III) complexes	14
2.3 Triplet-singlet energy transfer	16
2.4 Device performance	18
2.5 Morphological study	23
2.6 Compatibility studies of Ir(III) complexes in high-crystallinity polymer P3HT	27
2.7 Conclusion	30
III. Experimental Method and Materials	31
3.1 Synthesis of Ir(III) complexes	31
3.2 Fabrication of inverted PSCs	34
3.2.1 Device with PTB7	34
3.2.2 Device with P3HT	35
3.3 Morphological study	35
References	36
Acknowledgement	39

List of Figures

Figure 1.1 Structure and schematic mechanism of heterojunction and bulk-heterojunction solar cells.

Figure 1.2 Structures of PSCs.

Figure 1.3 (a) Energy level of each layer, (b) Schematic diagram of PSCs working mechanism.

Figure 1.4 A typical *J-V* curve of PSCs.

Figure 1.5 Structures of various donor and acceptor materials.

Figure 1.6 Structures of various donor materials applied in multi donor system.

Figure 1.7 Structures of donor and non-fullerene acceptor materials.

Figure 1.8 Structures of energy donor and acceptor materials.

Figure 1.9 Schematic mechanism of energy transfer.

Figure 1.10 Ideal spectra of energy donor and energy acceptor.

Figure 1.11 (a) Typical structures of Ir(III) complexes, (b) Energy state in Ir(III) complexes.

Figure 1.12 Structures of ligand for red, green and blue emitting Ir(III) complexes.

Figure 2.1 Synthetic routes of Ir(III) complexes.

Figure 2.2 (a) Chemical structures of Ir-Red, Ir-Orange, Ir-Green, Ir-Blue, PTB7, P3HT and PC₇₁BM. (b) Absorption (solid symbols; red square with line for Ir-Red, orange circle with line for Ir-Orange, green up-triangle with line for Ir-Green, and blue down-triangle with line for Ir-Blue) and PL (open symbols) spectra of the various Ir(III) complexes.

Figure 2.3 Absorption spectra of PTB7, absorption and emission spectra of (a) Ir-Red, (b) Ir-Orange, (c) Ir-Green, and (d) Ir-Blue.

Figure 2.4 (a) PL spectra of Ir-Orange with (open black diamond with line) and without (solid orange square with line) PTB7, and only PTB7 (solid black diamond) in film state. The magnified spectrum at 700–850 nm is shown in the inset. (b) Transient PL spectra of Ir-Orange with (orange line) and without (black line) PTB7 in film state.

Figure 2.5 Exciton lifetime of pristine Ir(III) complexes film and PTB7 blended film. Black line is transient PL spectra of (a) Ir-Red, (b) Ir-Orange, (c) Ir-Green, and (d) Ir-Blue and red, orange, green, and blue line is transient PL spectra of PTB7 blended film with (a) Ir-Red, (b) Ir-Orange, (c) Ir-Green, and (d) Ir-Blue, respectively.

Figure 2.6 (a) Structure of PSC. (b) Energy diagram of PSC with Ir(III) complexes. (c) $J-V$ curves of the PTB7-based PSC device with (orange circle with line) and without (black square with line) 10 wt% Ir-Orange under 1000 Wm^{-2} . (d) EQE spectra of the PSC device with (orange circle with line) and without (black square with line) 10 wt% Ir-Orange.

Figure 2.7 (a), $J-V$ curves of the device with 10wt% of various Ir(III) complexes under 1000 Wm^{-2} and (b), EQE data of devices with 10wt% various Ir(III) complexes

Figure 2.8 Efficiency of devices with Ir(III) complexes (black line) and FRET radius (red line).

Figure 2.9 Device performances, $J-V$ curves of reference, with Orange inserted layer, and with Orange in active layer.

Figure 2.10 2D GI-WAXD patterns of (a) PTB7, (b) PTB7:Ir-Red (10:1), (c) PTB7:Ir-Orange (10:1), (d) PTB7:Ir-Green (10:1), and (e) PTB7:Ir-Blue (10:1). (f) Chemical structures of the incorporated fluorine substituents of Ir-Blue and the thiophene spacers of PTB7. GI-WAXD line-cut profiles of (g) the PTB7:Ir(III) complex system, in-plane. Black square with line: PTB7. Red circle, orange up-triangle, green down-triangle, and blue diamond with line are for Ir-Red, Ir-Orange, Ir-Green, and Ir-Blue with PTB7 respectively. (h) PTB7:Ir(III) complex system, out-of-plane.

Figure 2.11 2D GI-WAXD patterns and line-cut profiles of PTB7:Ir(III) complex:PC₇₁BM blended films on ZnO modified Si substrate. (a) 2D GI-WAXD patterns of PTB7:PC₇₁BM (1:1.5), (b) PTB7:Ir-Red:PC₇₁BM (1:0.1:1.5), (c) PTB7:Ir-Orange:PC₇₁BM (1:0.1:1.5), (d) PTB7:Ir-Green:PC₇₁BM (1:0.1:1.5), (e) PTB7:Ir-Green2:PC₇₁BM (1:0.1:1.5), (f) PTB7:Ir-Blue:PC₇₁BM (1:0.1:1.5). GI-WAXD line-cut profiles of PTB7:Ir(III) complex:PC₇₁BM system (in-plane, g) and PTB7:Ir(III) complex:PC₇₁BM system (out-of-plane, h). (i) Structure of Ir-Green and Ir-Green2.

Figure 2.12 (a) 2D AFM image of PTB7:PC₇₁BM blended film, (b) 2D AFM image of PTB7:PC₇₁BM blended film with Ir-Green, (c) 2D AFM image of PTB7:PC₇₁BM blended film with Ir-Green2.

Figure 2.13 Overlap between emission of Ir(III) complexes and absorption of P3HT.

Figure 2.14 Device performance, J-V curves of P3HT reference, Ir-Orange in active layer and Ir-Blue in active layer

Figure 2.15 (a) 2D GI-WAXD patterns of P3HT, (b) P3HT:Ir-Orange (10:0.05), (c) P3HT:Ir-Blue (10:0.05), (d) P3HT:PC₆₁BM (10:8), (e) P3HT:Ir-Orange:PC₆₁BM (10:0.05:8), (f) P3HT:Ir-Blue:PC₆₁BM (10:0.05:8). GI-WAXD line-cut profiles of P3HT:Ir(III) complexes system (in-plane, g), P3HT:Ir(III) complexes system (out-of-plane, h), P3HT:Ir(III) complexes:PC₆₁BM system (in-plane, i), and P3HT:Ir(III) complexes:PC₆₁BM system (out-of-plane, j).

Figure 3.1 IR spectrum of (1pq)₂Irpic-OH (Ir-Red) in KBr pellet.

Figure 3.2 ¹H NMR of (1pq)₂Irpic-OH (Ir-Red) in CDCl₃.

Figure 3.3 ¹³C NMR of (1pq)₂Irpic-OH (Ir-Red) in CDCl₃.

List of Tables

Table 2.1 Optical properties, electrochemical properties, QY values of Ir(III) complexes.

Table 2.2 Exciton lifetime and calculated energy transfer efficiency of each Ir(III) complexes with and without PTB7 as an energy acceptor measured by transient PL.

Table 2.3 FRET radii, and device performances for the Ir(III) complexes.

Table 2.4 Summary of device performances with 5wt%, 10wt% and 15wt% of Ir-Orange.

Table 2.5 2D GI-WAXD parameters of the PTB7:Ir(III) complex:PC₇₁BM blended systems.

Table 2.6 Optical properties, electrochemical properties, QY values, FRET radii, and device performances for the Ir(III) complexes.

Table 2.7 Summary of device performances with Orange under 463nm and 200Wm⁻².

I. Introduction

1.1 Polymer solar cells (PSCs)

1.1.1 Development of PSCs

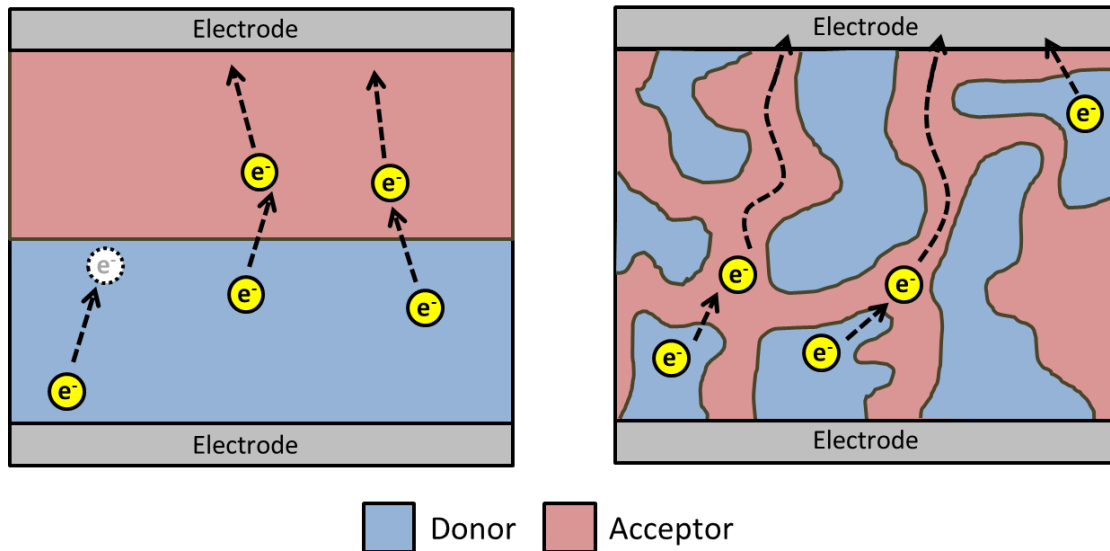


Figure 1.1 Structure and schematic mechanism of heterojunction and bulk-heterojunction solar cells.

The first solar cells were silicon based solar cells (Si cells) and it was invented from Bell Lab in 1954. After some decades these Si cells are commercialized. However, due to the nature of silicon wafer, Si cells require high cost and its appearance is just black and non-transparent. Also, Si cells are rigid and not flexible. To solve these problems of Si cells, the polymer solar cells (PSCs) can be an answer.

The earlier type of PSCs is heterojunction (HJ) type. As shown in Figure 1.1, the HJ cells have two layers consist of donor and acceptor material. When the donor absorbs light, the electrons are excited and the excited electrons are transported to acceptor layer. The electrons in acceptor layer are collected to the electrode to generate photocurrent. However, the diffusion length of electron is not long enough to move through thick bilayers. The thicker layer is necessary to absorb more light, but in thick layered device, the electrons are not able to be converted to current.

To solve this problem of HJ type cells, new type of structure is developed. Bulk-heterojunction (BHJ)

structure has mono layer of donor-acceptor mixture (Figure 1.1). In the BHJ layer, the donor and acceptor materials are mixed with each other. Therefore, when electrons of donor are excited, the electrons can be easily transported to acceptor and can be easily collected to electrode to generate photocurrent. Although the donor-acceptor layer becomes thicker, the electrons can be converted to current in BHJ cells. After BHJ type is developed, the typical PSCs have BHJ structure.

1.1.2 Structure and mechanism of PSCs

The PSCs are the solar cells fabricated with conductive polymers and the structure of PSCs is shown in Figure 1.2. The PSCs are consisted of transparent conducting oxide materials as photoelectrode, electron transporting layer (ETL) for easier electron transport, photoactive layer to generate current, hole transporting layer (HTL) for easier hole transport and metal anode. As shown in Figure 1.3, the electron and hole, which are generated at the photoactive layer, are transported through these layers and finally the photocurrent is generated. When the donor material absorbs light, the electron is excited. The excited electron is moving through acceptor and ETL to the anode and the hole is moving though HTL to the cathode, then the electron of donor material can be regenerated.

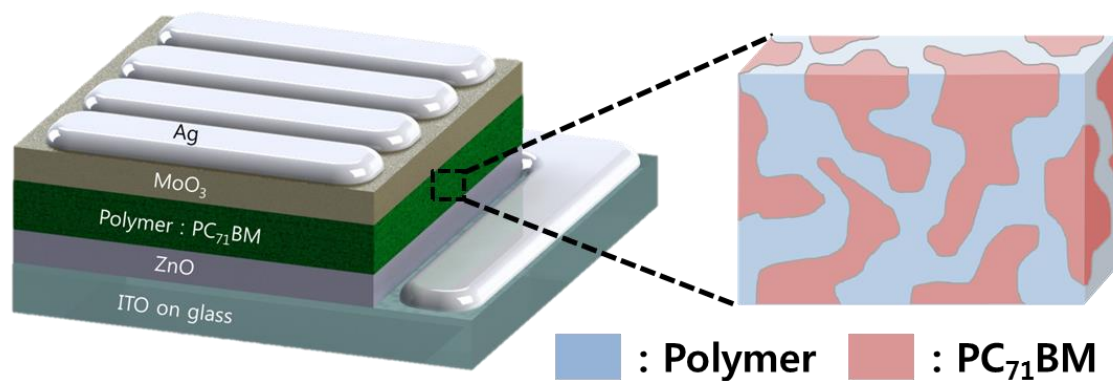


Figure 1.2 Structures of PSCs.

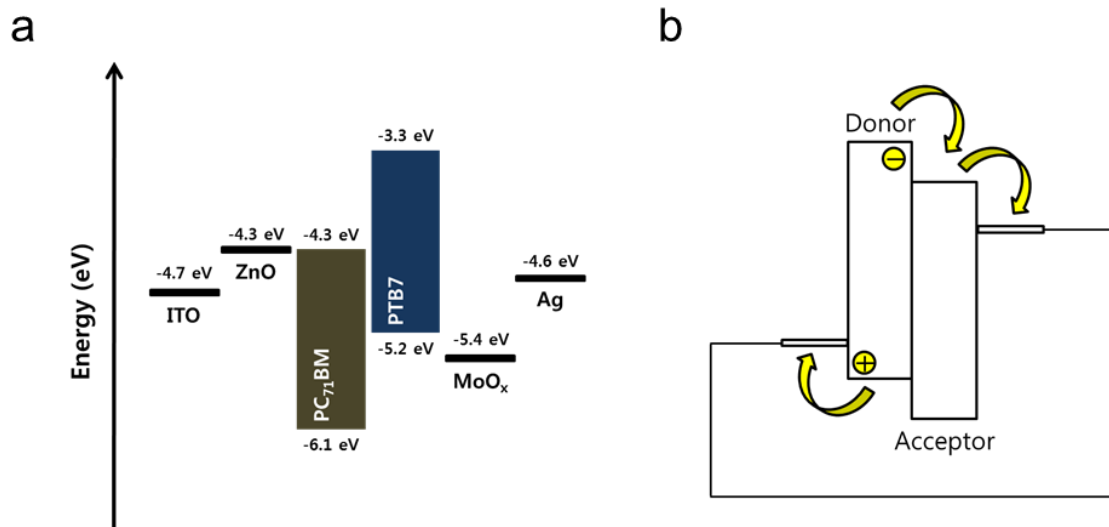


Figure 1.3 (a) Energy level of each layer, (b) Schematic diagram of PSCs working mechanism.

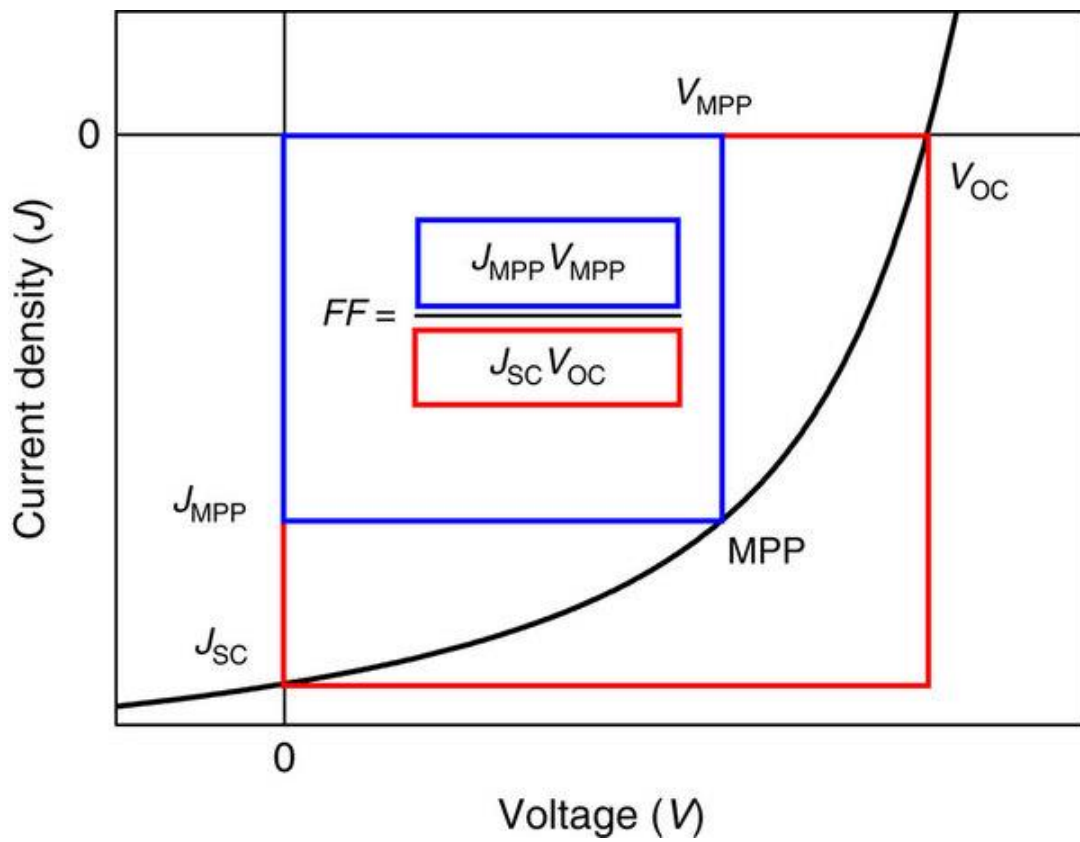


Figure 1.4 A typical J - V curve of PSCs.

1.1.3 Characterization of PSCs

To evaluate the performance of PSCs, J - V is utilized. To get the J - V curve, the flow of current is analyzed under sweeping bias from backward to forward. With J - V curve, the short-circuit current density (J_{SC}), open-circuit voltage (V_{OC}) and fill factor (FF) can be acquired.

Here, as shown in Figure 1.4, J_{SC} is the current density when the voltage is zero. The current density with zero bias is the current density of the device. The V_{OC} is the voltage when the current is zero. The V_{OC} corresponds to the amount of forward bias on the solar cell due to the bias of the solar cell junction with the light-generated current. Finally, the efficiency (η) of PSCs is calculated by the equation:

$$\eta = FF \frac{J_{SC} V_{OC}}{P} \quad (1)$$

1.2 Trends of research in PSCs

PSCs are flexible, lightweight, and highly customizable, but their efficiency is still lower than that of silicon-based cells. A broad spectral absorption range is critical for high-efficiency PSCs that consist of a polymer donor material and fullerene acceptor. However, single-donor materials show limited generation of photocurrent and a narrow absorption region across the solar spectrum. Therefore, many researchers have studied about strategies based on multiple donors and energy transfer systems.

1.2.1 Single donor system

The single donor system is the simplest system of PSCs. In 1995, the first PSC was reported.¹ They used MEH-PPV as a donor, C_{60} as an acceptor and the efficiency was 2.9%. After this paper, development of new donor polymer for PSCs becomes hot issue and many polymers with high performance have developed. After MEH-PPV, new polymer (P3HT) was reported.² For few years, the P3HT was the most popular donor material for researchers. To enhance the performance of P3HT based device, new kind of acceptor ($IC_{71}BA$) is also developed.³ As a result, 5.8% of efficiency is achieved with P3HT and $IC_{71}BA$.

In the solar spectrum, near-IR region is wider than short wavelength region. For higher efficiency, the single donor materials have been developed for broader absorption. For broader absorption, the polymer donors should have longer conjugation length or narrower energy band gap. In 2010, new polymer named PTB7 was reported. The efficiency of PTB7/ $PC_{71}BM$ based cell was 7.4% and it was very successful.⁴ After the PTB7 was reported, for few year, the PTB7 replaced the P3HT in research

of PSCs. When PTB7 was reported, many researchers tried to develop a donor material beyond PTB7. And then, the PTB7-modified polymer named PTB7-Th was reported in 2015.⁵ The new polymer, PTB7-Th, shows over 10% of efficiency (10.6%). The PTB7-Th absorbs longer wavelength light than PTB7 and this is the point for higher performance. Until now, the best performance with single donor material is over 11%. The polymer named PffBT4T-2OD was used as donor.⁶ However, it is limited to increase conjugation length or to decrease energy band gap of polymer donor materials and because of these problem, multi donor system has been researched. The above donor and acceptor materials are shown in Figure 1.5.

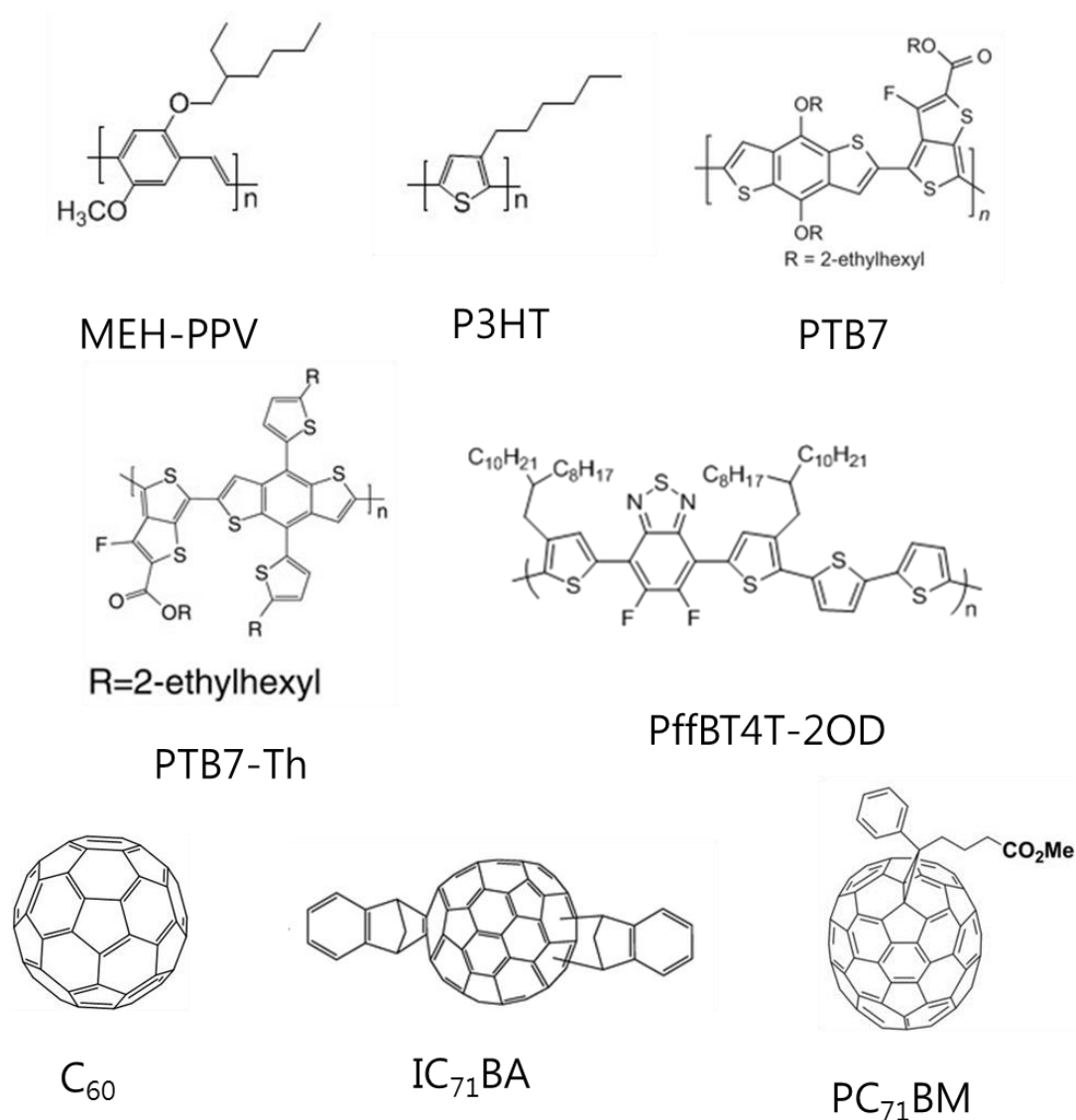


Figure 1.5 Structures of various donor and acceptor materials.

1.2.2 Multi donor system

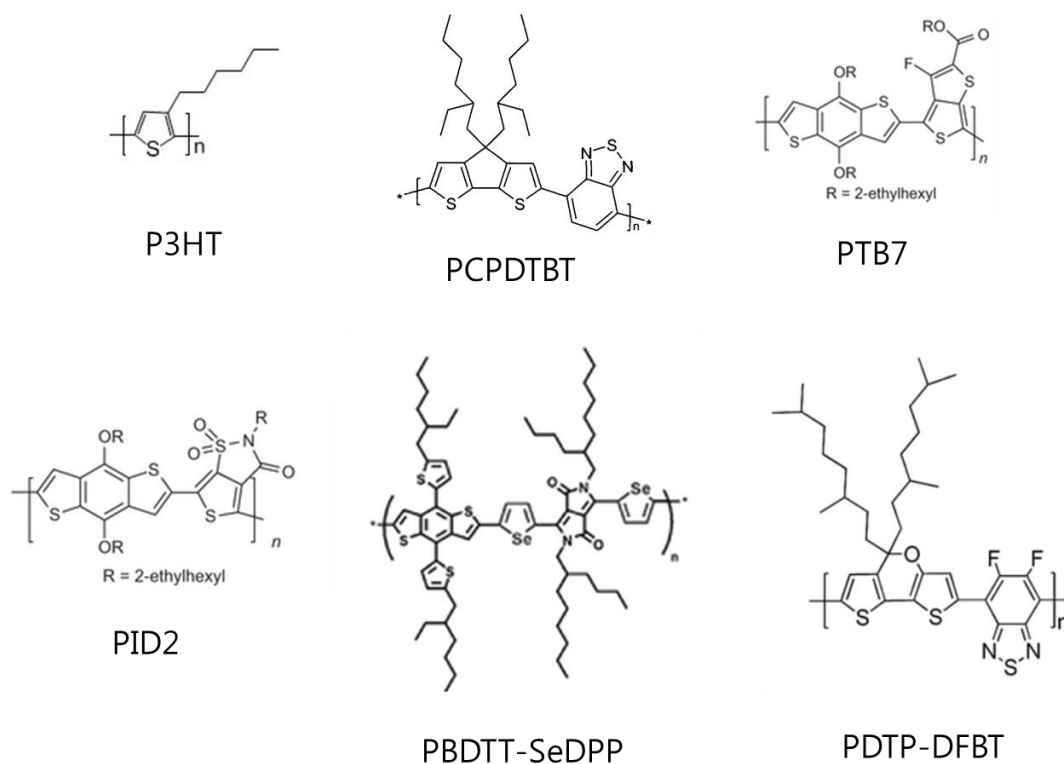


Figure 1.6 Structures of various donor materials applied in multi donor system.

For the better performance of PSCs, broader absorption is a key point. Due to the limitation of single donor system, the multi donor system has been researched. This system uses two different polymers as donor materials and these two polymers absorb different region of solar spectrum. With ternary systems, the absorption range increased because of compensative absorption range of multi donors.

The first multi donor system was reported in 2010.⁷ Two polymers, P3HT and PCPDTBT were used as multi donor materials. The PCPDTBT has absorption range in long wavelength region. Therefore the total absorption range of blended film became broader. Also, the efficiency of device was enhanced. After the multi donor system was reported, many studies about multi donor system are reported with P3HT. However, due to the low efficiency of P3HT, those multi donor systems which based on P3HT shows low performances less than 5%.⁸

To raise a performance of PSCs with multi donor systems, the PTB7 was applied at multi donor system. In 2014, a research with PTB7 and PID2 showed 8.2% of efficiency.⁹ Also, in 2015, with

PTB7 and PBDTT-SeDPP, 8.7% of efficiency was reported.¹⁰ In 2016, similar research with PTB7 and PDTP-DFBT showed 8.6% of efficiency.¹¹ However, due to these systems are using polymer-polymer system, the molecular compatibility in such systems remains difficult to control, given that the polymers can exhibit different crystallinities and energy levels, thereby making it challenging to ensure efficient charge transfer. To overcome the compatibility problem, new type (non-fullerene) of acceptors has been researched. The above donor materials are shown in Figure 1.6.

The above existing researches applied fullerene derivatives as acceptor materials but most of them absorbs short wavelength region. Unlike them, new acceptors absorb compensative region with polymer donors. Thus, the new acceptors can also work as a multi donor material. In the early days of non-fullerene acceptors, the performance was very low. However, in 2016, 8.3% of efficiency was reported with J51 donor and N2200 acceptor.¹² The absorption range of N2200 can compensate the absorption range of J51. The N2200 brought an effect of multi donor system with only one donor material, because of wide absorption of acceptor material. Also, in 2016, 9.5% was reported with J61 donor and ITIC acceptor.¹³ The absorption of ITIC can compensate the absorption range of J61 and as a result, high performance was achieved. The most recent and the best record is over 11% (11.2%) of efficiency with PBDB-T donor and ITIC acceptor.¹⁴ The new type of acceptor is simple and strong way to enhance performance with broadening absorption range. The above donor and acceptor materials are shown in Figure 1.7.

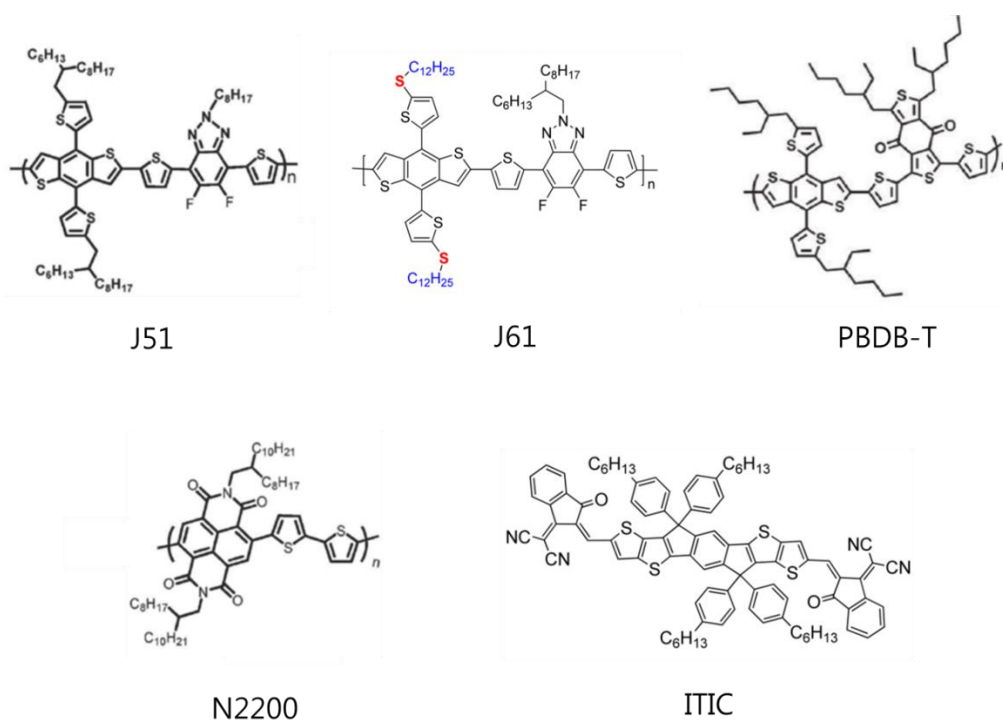


Figure 1.7 Structures of donor and non-fullerene acceptor materials.

1.2.3 Energy transfer system

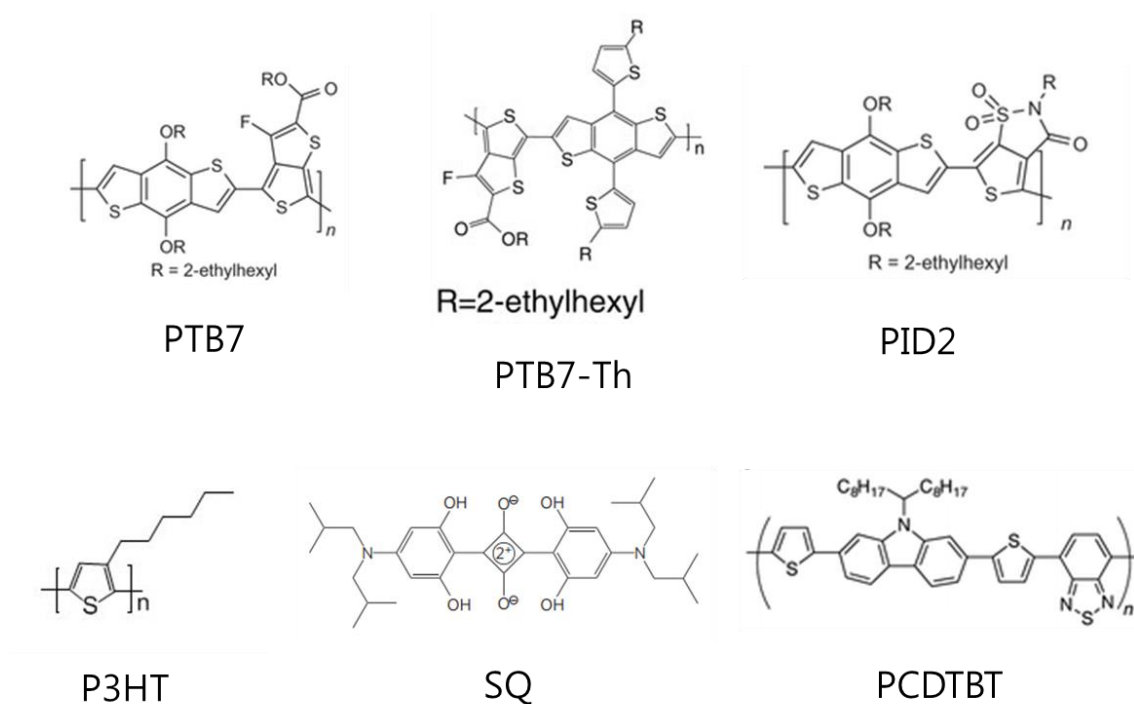


Figure 1.8 Structures of energy donor and acceptor materials.

Single and multi-donor systems are based on charge transfer. Not only charge transfer system, the energy transfer can be another strategy to broaden the absorption range of PSCs. For the energy transfer, energy donor and energy acceptor materials are needed. Unlike multi donor system, the energy donor does not generate electron directly and they transfer their absorbed energy to the energy acceptor. During this mechanism, the energy acceptor can generate more electrons with transferred energy from energy donor. Actually, there are some researches of energy transfer system in PSCs.

The first paper applied energy transfer was reported in 2013.¹⁵ The P3HT was used as an energy donor and SQ was used as acceptor. The absorption range of SQ is in longer wavelength region than P3HT. Thus, with SQ, the overall absorption increased and the performance was enhanced. The absorbed light energy by P3HT is transferred to SQ, and then the amount of electrons generated by SQ increased. By this mechanism, the efficiency was enhanced from 3.3% to 4.5%. However, due to low performance of P3HT, further researches about energy transfer applied PTB7 and PTB7-Th based PSCs.

In 2015, energy transfer system with PTB7-Th was reported.¹⁶ In this system, the PID2 was used for energy donor and PTB7-Th was used as energy acceptor. Because the energy band gap of PTB7-Th is narrower than PTB7, the energy transfer was dominant between PID2 and PTB7-Th. By the energy transfer, the total absorption of blended film was broadened. As a result, the performance was enhanced from 7.9% to 9.2%. Also in 2015, another energy transfer system with PTB7 was reported.¹⁷ In this system, the PCDTBT was used for energy donor and PTB7 was used for energy acceptor. Similar to the previous research, the performance was enhanced (6.8% to 8.9%) with broadened absorption range. In these researches, the authors proved that the energy transfer is another strategy to enhance absorption range and performance of PSCs. The above energy donor and acceptor materials are shown in Figure 1.8.

1.3 Energy transfer

1.3.1 Mechanism

Energy transfer is one of the ways to broaden the absorption range to enhance performance of PSCs. It is necessary to occur energy transfer, energy donor and energy acceptor. When electrons in the energy donor get back to ground state from its excited state, the energy is emitted. Then electrons of the energy acceptor can be excited by absorbing the energy from energy donor. This phenomenon is called energy transfer.

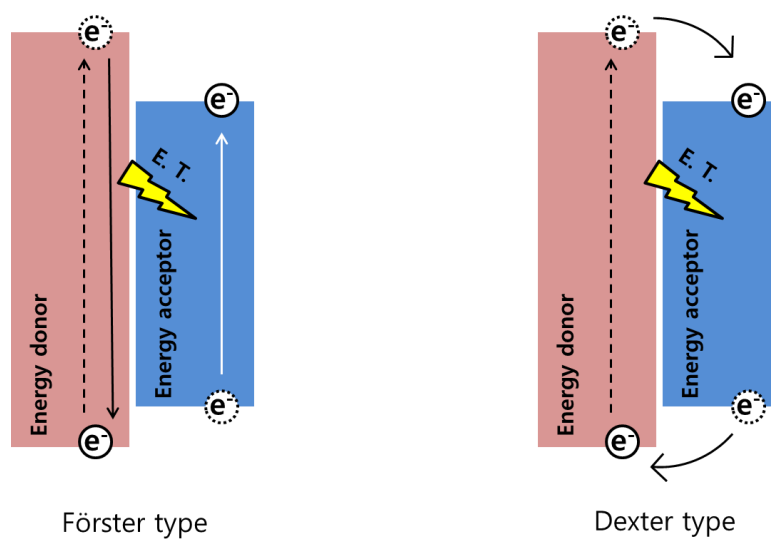


Figure 1.9 Schematic mechanism of energy transfer.

There are two types of energy transfer, Förster type and Dexter type energy transfer. Förster energy transfer is singlet-singlet transfer and dipole-dipole interaction between donor and acceptor. The energy transfer radius is about 10 nm. Unlike Förster type, Dexter energy transfer is singlet-singlet or triplet-triplet electron exchange between donor and acceptor. Thus the energy transfer radius is 1 nm, much shorter than Förster type.

1.3.2 Conditions for efficient energy transfer

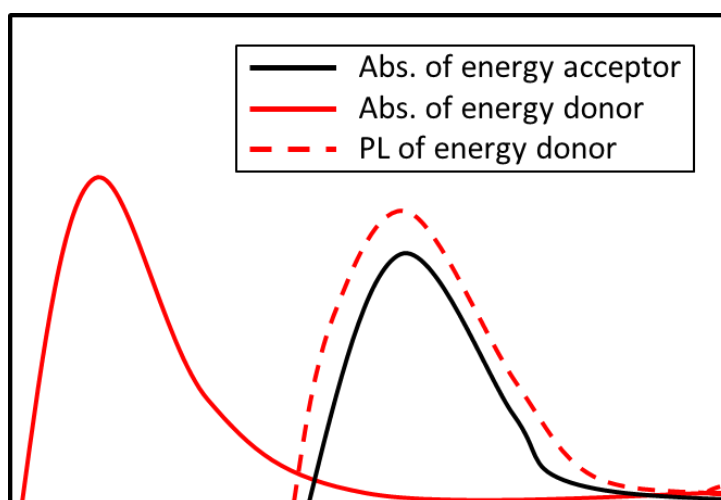


Figure 1.10 Ideal spectra of energy donor and energy acceptor.

For efficient energy transfer, five conditions are needed to energy donor (Figure 1.9 and 1.10). The high quantum yield (QY) is needed to reduce energy loss occurs in energy donor. Large Stokes shift is also needed for energy donor to prevent self-quenching occurs in energy donor. For efficient energy transfer, it is necessary that the large amount of spectral overlap between absorption of energy acceptor and emission of energy donor. At last, energy donor should have wider energy band gap than energy acceptor to avoid charge transfer between energy donor and acceptor.

1.4 Iridium complexes

The iridium complexes (Ir(III) complexes, Figure 1.11 a) are usually applied in organic light emitting diodes or bio imaging because of its high QY. As shown in Figure 1.11b, unlike other light emitting materials, Ir(III) complexes emit phosphorescence. The phosphorescence is emitted when the electron

on triplet state is dropped to ground state. In case of typical fluorophores, the electron on triplet state is dropped to ground state by non-radiative decay. However, Ir(III) complexes can emit light from both singlet and triplet state and this is the reason of high QY. Also, the phosphorescence of Ir(III) complexes is came from metal-to-ligand charge transfer (MLCT) state (Figure 1.11b). Generally, phosphorescence materials show large Stokes shift. The energy band gap between MLCT to ground state is narrower than gap of singlet to ground state. Because of this difference in energy band gap, an emission wavelength shows large red shift compare to absorption wavelength and this shifting phenomenon is called Stokes shift.

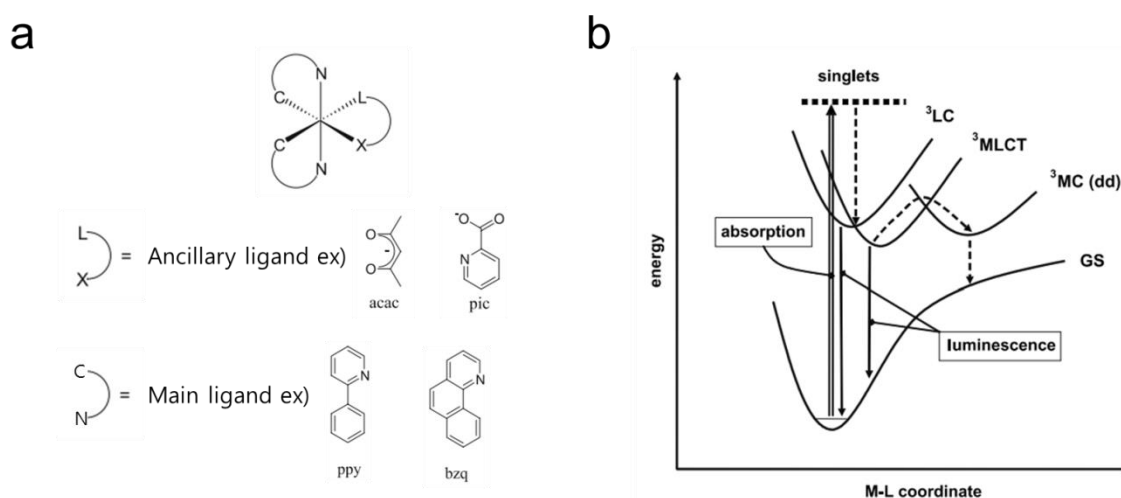


Figure 1.11 (a) Typical structures of Ir(III) complexes, (b) Energy state in Ir(III) complexes.

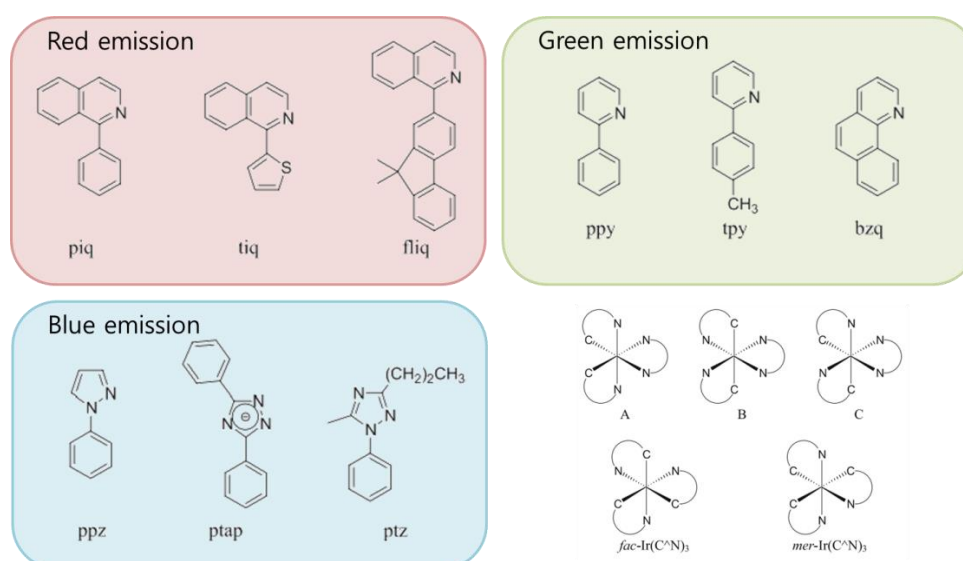


Figure 1.12 Structures of ligand for red, green and blue emitting Ir(III) complexes.

The absorption and emission is decided by energy states in Ir(III) complexes. The energy states of Ir(III) complexes are decided by ligands. Therefore the optical properties of Ir(III) complexes can be easily controlled by its ligands. Actually, there are plenty of ligands developed for color tuning of Ir(III) complexes (Figure 1.12). The existing Ir(III) complexes can emit most of colors in visual light and further more preparing new Ir(III) complexes that have necessary emission range. In Figure 1.11a, the Ir(III) complexes have two main ligands and one ancillary ligand. The photophysical properties of Ir(III) complexes are determined by main ligands and ancillary ligand barely affect to the optical properties. Therefore, it is possible to functionalize the Ir(III) complexes with ancillary ligand.

In this study, for the first time, we developed customized energy transfer materials for both amorphous and high crystalline polymer materials and then investigated a triplet-singlet energy transfer system for enhanced performance of PSCs, instead of the conventional singlet-singlet energy transfer system. Triplet systems have several advantages, such as a larger Stokes shift to prevent self-quenching, a larger diffusion length, and reduced charge recombination compared to singlet systems. With this aim in mind, we used iridium-based energy donors customized for two representative active polymer materials: the amorphous PTB7, and the high-crystallinity P3HT. The Ir(III) complexes are used as energy donors since they exhibit a number of additional advantages, such as high QY and easy control of the energy levels and molecular compatibility. As a result, customizable Ir(III) complexes perfectly satisfy these prerequisites of an energy donor.

II. Result and Discussion

2.1 Synthesis of iridium (Ir(III)) complexes

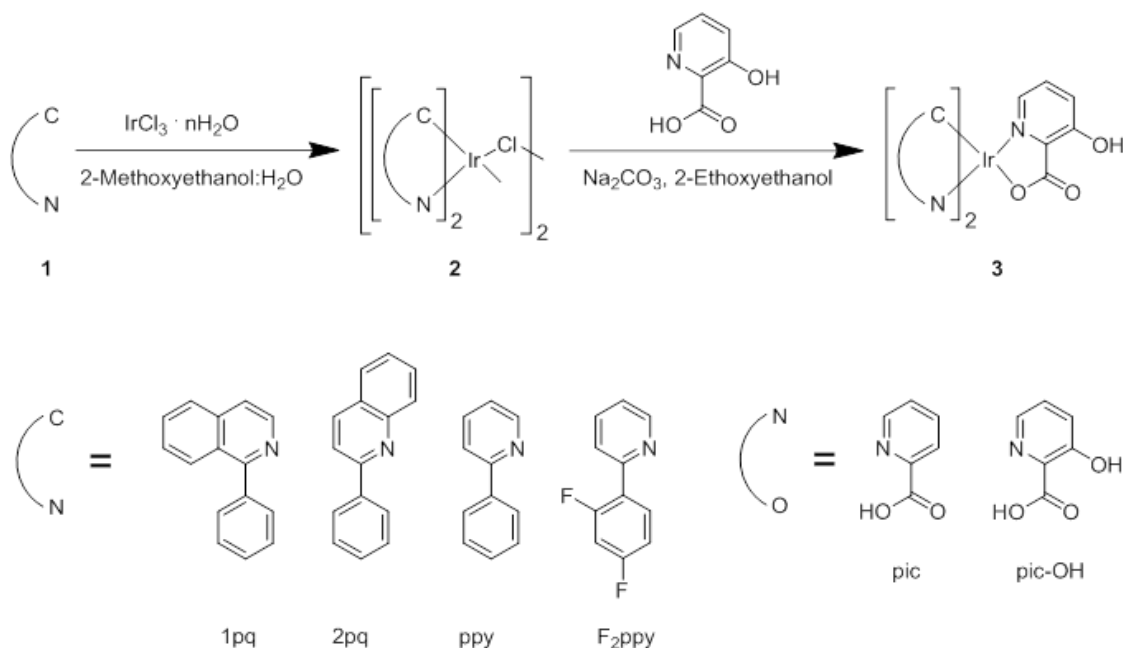


Figure 2.1 Synthetic routes of Ir(III) complexes.

The route employed to synthesize the four Ir(III) complexes used in this study is depicted in Figure 2.1; the experimental details are given in Experimental Section (with spectra characterization of Ir-Red). To control the absorption and emission characteristics of the Ir(III) complexes, four different hydrophobic primary ligands (Figure 2.2) were used: 1-phenylisoquinoline (1pq), 2-phenylquinoline (2pq), phenylpyridine (ppy), and difluorophenylpyridine (F_2ppy). These ligands have been shown to be high-QY materials when incorporated with iridium.¹⁸⁻²¹ They also exhibit emissions of different colors, which range from blue, green, and orange to red, as the conjugation length is increased. Hydrophilic 3-hydroxypicolinic acid (pic-OH) was introduced as an ancillary ligand for controlling the molecular compatibility.²² The material (ppy)₂Irpic (Ir-Green2) with picolinic acid was also used to study the effect of the hydroxyl group of pic-OH. We observed an improvement in the active layer morphology due to the amphiphilic nature of the Ir(III) complexes, using grazing incidence-wide angle X-ray diffraction (GI-WAXD) analysis and atomic force microscopy (AFM). This phenomenon is discussed further in the subsection titled Morphological study.

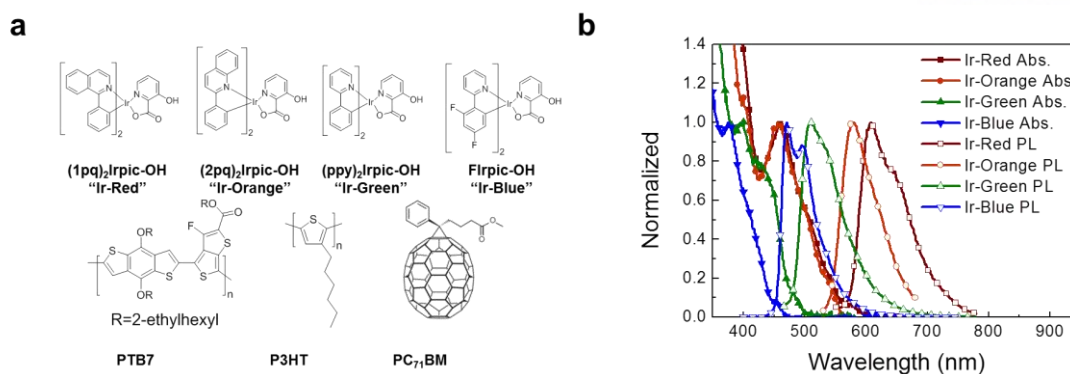


Figure 2.2 (a) Chemical structures of Ir-Red, Ir-Orange, Ir-Green, Ir-Blue, PTB7, P3HT and PC₇₁BM. (b) Absorption (solid symbols; red square with line for Ir-Red, orange circle with line for Ir-Orange, green up-triangle with line for Ir-Green, and blue down-triangle with line for Ir-Blue) and PL (open symbols) spectra of the various Ir(III) complexes.

2.2 Photophysical and electrochemical studies of Ir(III) complexes

Table 2.1 and Figure 2.2b show the absorption and emission properties of the developed Ir(III) complexes. The absorption spectra of the Ir(III) complexes in the film state indicate a π - π^* ligand-centered transition at wavelengths lower than 350 nm. Ir-Blue, Ir-Green, Ir-Orange, and Ir-Red exhibited MLCT at 376, 400, 455, and 462 nm, and the corresponding maximum emission peaks (λ_{max}) appeared at 471, 511, 580, and 608 nm, respectively. All the Ir(III) complexes exhibited large Stokes shifts at wavelengths higher than 100 nm, which prevented self-quenching.²³ Figure 2.3 depicts the overlapping between the emission spectra of the iridium-based energy donors and the absorption spectrum of PTB7. The degree of spectral overlap, which is one of the most important factors for efficient energy transfer, follows the order Ir-Red > Ir-Orange > Ir-Green > Ir-Blue. The QY values of the Ir(III) complexes measured in a CH₂Cl₂ solution are ordered as follows: Ir-Orange (0.23) > Ir-Blue (0.21) > Ir-Red (0.12) > Ir-Green (0.06) (Table 2.1). The QY value also affects energy transfer, and the values obtained are discussed below on the basis of a device study. The energy levels of the highest occupied molecular orbitals (HOMO, -5.44 to -5.73 eV) and lowest unoccupied molecular orbitals (LUMO, -3.19 to -2.94 eV) of the Ir(III) complexes included the energy level of PTB7 (HOMO = -5.15 eV, LUMO = -3.31 eV) and P3HT (HOMO = -5.20 eV, LUMO = -3.21 eV), as shown in Table 2.1. These results indicate that efficient energy transfer occurred from the energy donor to the acceptor.

Table 2.1 Optical properties, electrochemical properties, QY values of Ir(III) complexes.

PTB7_Ir(III) complexes	UV (nm)	PL (nm)	HOMO (eV)	LUMO (eV)	Bandgap (eV)	QY
PTB7_Ref.	-	-	-5.2	-3.3	1.9	-
PTB7_Ir-Red	462	608	-5.4	-3.2	2.2	0.12
PTB7_Ir-Green	400	511	-5.6	-2.9	2.7	0.06
PTB7_Ir-Blue	376	471	-5.7	-3.0	2.7	0.21
PTB7_Ir-Orange	455	580	-5.5	-3.2	2.3	0.23

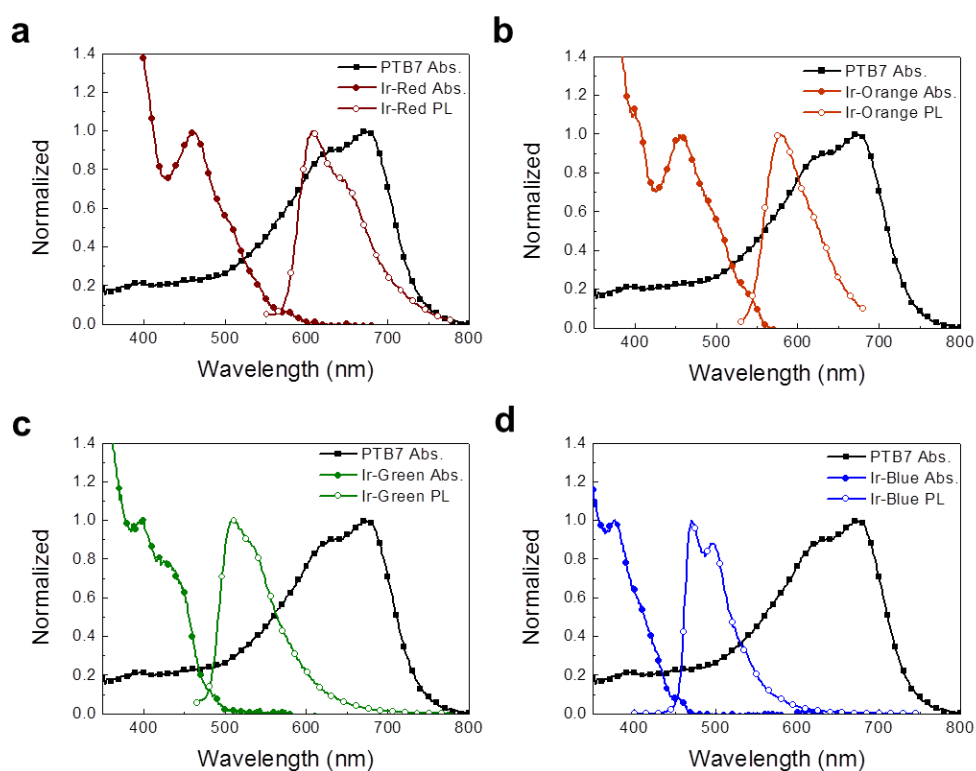


Figure 2.3 Absorption spectra of PTB7, absorption and emission spectra of (a) Ir-Red, (b) Ir-Orange, (c) Ir-Green, and (d) Ir-Blue.

2.3 Triplet-singlet energy transfer

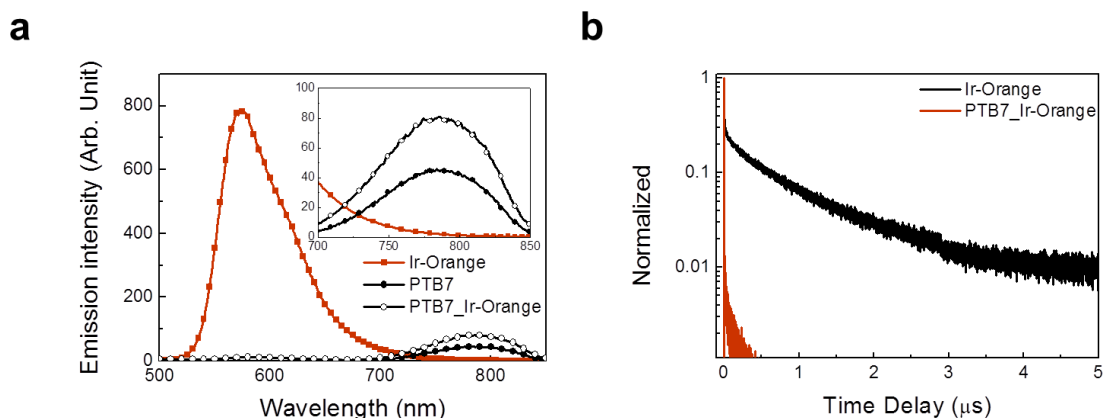


Figure 2.4 (a) PL spectra of Ir-Orange with (open black diamond with line) and without (solid orange square with line) PTB7, and only PTB7 (solid black diamond) in film state. The magnified spectrum at 700–850 nm is shown in the inset. (b) Transient PL spectra of Ir-Orange with (orange line) and without (black line) PTB7 in film state.

To confirm the transfer of energy from the iridium-based energy donors to the acceptor, both steady-state and transient photoluminescence (PL) spectroscopy were performed using time-correlated single photon counting. The PL intensity of PTB7 with 10 wt% Ir-Orange in the film state was twice that of intrinsic PTB7, while the emission of Ir-Orange almost disappeared when excited in the MLCT region (455 nm, Figure 2.4a). These results can be attributed to triplet-singlet energy transfer and not charge transfer. In addition, the reduction in the PL intensity of Ir-Orange was directly related to η_{ET} . By integrating the emission spectra of the Ir(III) complexes, their ET values were calculated to be 98%. The energy transfer efficiency is $(1 - A_{D-A}/A_D) \times 100(\%)$ measured from the steady-state PL method, where A_{D-A} is the total integral area of emission intensity of Ir-complex with PTB7, A_D is the total integral area of emission intensity of Ir-complex.²⁴

The η_{ET} value can be determined with accuracy by measuring the exciton lifetimes of the Ir(III) complexes using transient PL spectroscopy with and without PTB7. The η_{ET} value was calculated using the following formula²²:

$$\eta_{ET} = 1 - \frac{\tau_{A,D}}{\tau_D} \quad (2)$$

where $\tau_{A,D}$ and τ_D are the exciton lifetimes of the energy donor Ir(III) complexes with and without the

energy acceptor (PTB7), respectively. The obtained results are shown in Table 2.2. The pristine lifetimes of the Ir(III) complexes were as follows: 859 ns for Ir-Red, 1236 ns for Ir-Orange, 1466 ns for Ir-Green, and 1929 ns for Ir-Blue. The longer exciton lifetimes compared to those of polymers helped in increasing the FRET radius, resulting in an increased η_{ET} .¹⁷ When the Ir(III) complexes were used with PTB7, their exciton lifetimes excited in the MLCT region decreased dramatically: 9 ns for Ir-Red, 14 ns for Ir-Orange, 77 ns for Ir-Green, and 90 ns for Ir-Blue (Figure 2.4b and 2.5). These correspond to the η_{ET} values of 99%, 99%, 95%, and 95%, respectively. A sharp decrease in the lifetime of the energy donor is characteristic of energy transfer,²⁴ and all the iridium-based energy donors studied here exhibited high η_{ET} values (>95%). This was in keeping with the values obtained using steady-state PL spectroscopy.

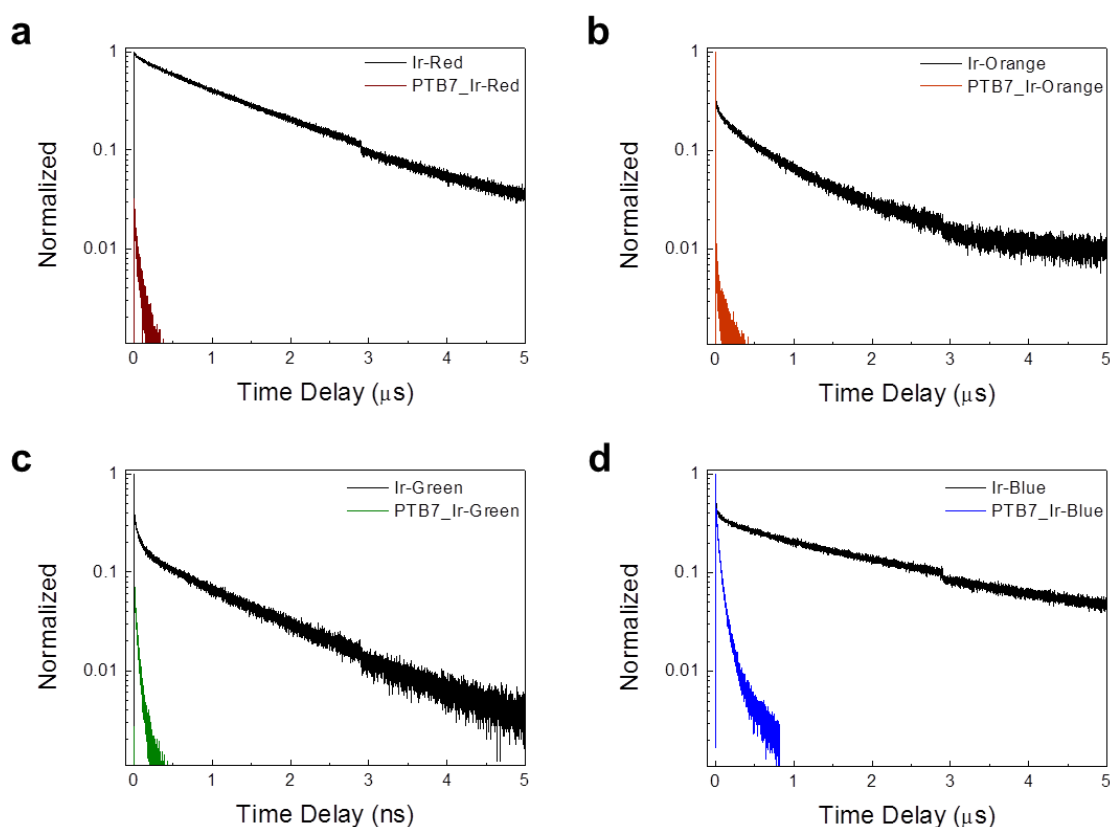


Figure 2.5 Exciton lifetime of pristine Ir(III) complexes film and PTB7 blended film. Black line is transient PL spectra of (a) Ir-Red, (b) Ir-Orange, (c) Ir-Green, and (d) Ir-Blue and red, orange, green, and blue line is transient PL spectra of PTB7 blended film with (a) Ir-Red, (b) Ir-Orange, (c) Ir-Green, and (d) Ir-Blue, respectively.

Table 2.2 Exciton lifetime and calculated energy transfer efficiency of each Ir(III) complexes with and without PTB7 as an energy acceptor measured by transient PL.

Conditions	Ir-Red	Ir-Orange	Ir-Green	Ir-Blue
Ir(III) complex only	859 ns	1236 ns	1466 ns	1929 ns
Ir(III) complex with PTB7	9 ns	14 ns	77 ns	90 ns
η_{ET}	99%	99%	95%	95%

2.4 Device performance

Table 2.3 FRET radii, and device performances for the Ir(III) complexes.

PTB7_Ir(III) complexes	FRET radius (nm)	J_{sc} (mAcm ⁻²)	V_{oc} (V)	FF (%)	Best PCE (%)	Average PCE (%)
PTB7_Ref.	-	13.3	0.75	71.7	7.37	7.23 ± 0.14
PTB7_Ir-Red	7.8	15.9	0.74	72.4	8.53	8.41 ± 0.12
PTB7_Ir-Green	5.7	15.9	0.75	70.0	8.32	8.14 ± 0.18
PTB7_Ir-Blue	6.3	15.9	0.74	72.3	8.52	8.41 ± 0.11
PTB7_Ir-Orange	8.2	16.1	0.74	72.9	8.72	8.62 ± 0.10
PTB7_Ir-Orange (inserted layer)	-	13.3	0.75	69.9	7.23	7.03 ± 0.20

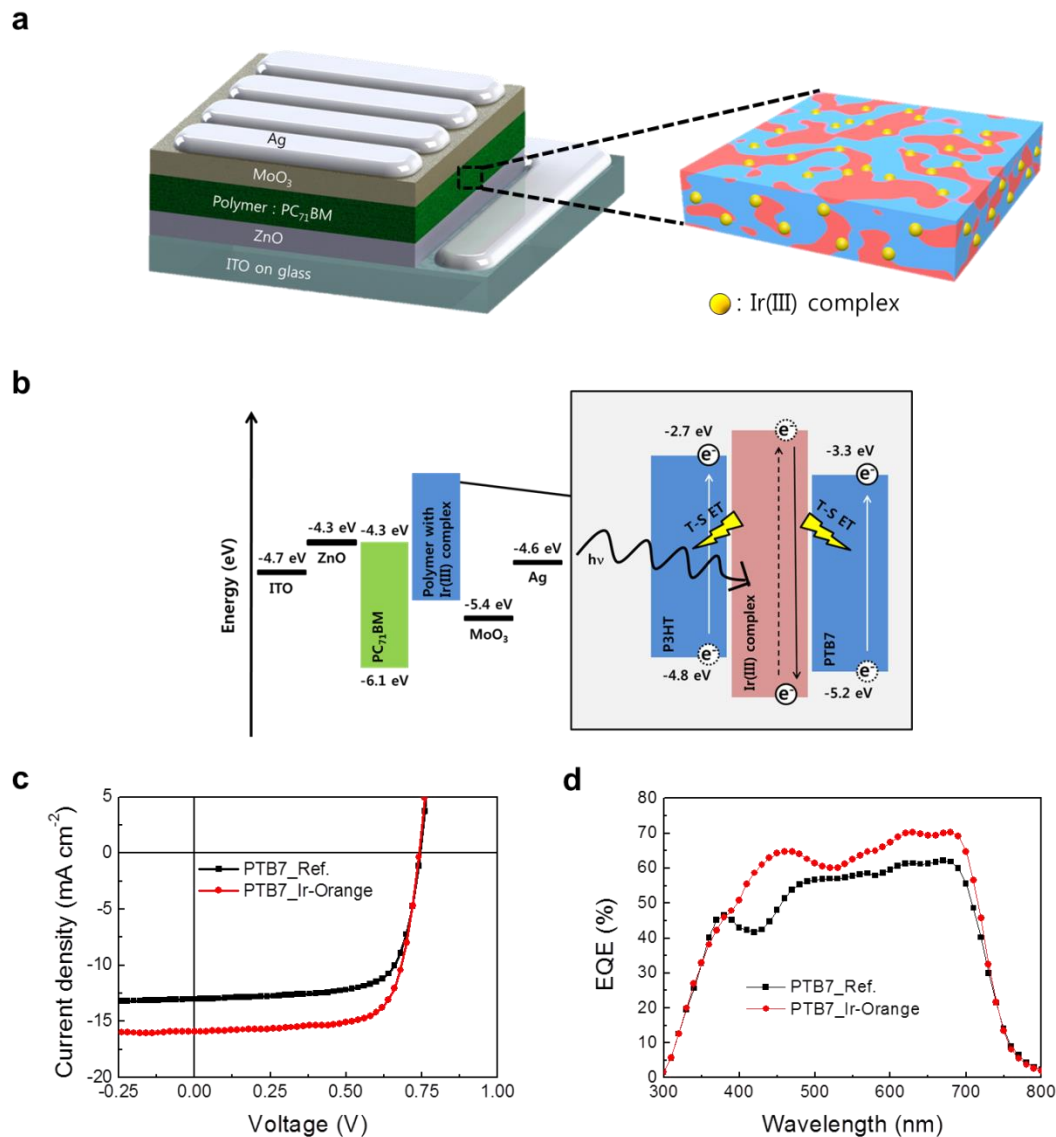


Figure 2.6 (a) Structure of PSC. (b) Energy diagram of PSC with Ir(III) complexes. (c) J - V curves of the PTB7-based PSC device with (orange circle with line) and without (black square with line) 10 wt% Ir-Orange under 1000 W m^{-2} . (d) EQE spectra of the PSC device with (orange circle with line) and without (black square with line) 10 wt% Ir-Orange.

Inverted PSCs were fabricated with the structure of glass/indium tin oxide (ITO)/zinc oxide (ZnO)/active layer/molybdenum trioxide (MoO_3)/Ag, as shown in Figure 2.6a and b. Table 2.3 shows the photovoltaic characteristics of these devices fabricated with and without the Ir(III) complexes, measured under AM1.5G illumination. Incorporating the four iridium-based energy donors in an optimized ratio of 10 wt% (see Table 2.4) in the PTB7:PC₇₁BM film led to significant enhancements

in the J_{SC} and thereby the PCE. In the device with 10 wt% Ir-Orange with respect to PTB7, $J_{SC} = 16.1$ mAcm^{-2} , open circuit voltage (V_{OC}) = 0.74 V, fill factor (FF) = 72.9%, and PCE = 8.72%. The J_{SC} and PCE values were 21% and 18% higher than those of the reference device from the current density-voltage (J - V) curves, respectively (Figure 2.6c and Table 2.3). The efficient energy transfer increased J_{SC} , as confirmed by the external quantum efficiency (EQE) spectra (Figure 2.6d). Specifically, the enhanced EQE peak was observed at 400–500 nm, which is the absorption range of the Ir-Orange complex. This directly proves that efficient energy transfer occurred between the iridium-based energy donor and the energy acceptor PTB7. The EQE spectrum was also enhanced for wavelengths greater than 500 nm, and this might be related to the improvement in the active layer morphology, or reduction of charge recombination by Ir(III) complexes.^{25,26} These will be discussed in the next subsection. When other iridium-based energy donors were incorporated in the PTB7:PC₇₁BM film, the PCEs of the resulting PSCs were 8.53% (Ir-Red), 8.52% (Ir-Blue), and 8.32% (Ir-Green), all of which still higher than that of the control device (Figure 2.7a). The corresponding EQEs matched well with the increase in the J_{SC} and were higher than that for the control device (Figure 2.7b). The amount of increased PCE values could be arranged in the following order: Ir-Orange > Ir-Red > Ir-Blue > Ir-Green. The fact that devices based on Ir-Orange exhibited the highest PCE can be explained by the η_{ET} value and the FRET radius. First, the η_{ET} value corresponding to energy transfer was the highest in the case of Ir-Orange (99% as calculated earlier). Second, Ir-Orange as energy donor exhibited the largest FRET radius R_0 (8.2 nm, Table 2.3), which was calculated using the following equation²⁷:

$$R_0 = \sqrt[6]{\frac{90000\kappa^2\eta_D \ln 10}{128\pi^5 n^4 N_A} \int_0^\infty f_d(\lambda)\epsilon_A(\lambda)\lambda^4 d\lambda} \quad (3)$$

where κ^2 is the dipole orientation factor, η_D is the QY value, n is the refractive index of the medium, N_A is Avogadro's number, $f_d(\lambda)$ is the normalized energy donor emission spectrum, $\epsilon_A(\lambda)$ is the molar extinction coefficient of the energy acceptor, and the integral represents the spectral overlap. Equation (3) suggests that the most important factors determining the FRET radius are QY and the degree of spectral overlapping. From Table 2.3, the FRET radius of each of the iridium-based energy donors is as follows: 8.2 nm for Ir-Orange, 7.8 nm for Ir-Red, 6.3 nm for Ir-Blue, and 5.7 nm for Ir-Green. These values correlate very well with the observed increases in the PCE (Figure 2.8). Although the FRET radius of Ir-Blue was much smaller than that of Ir-Red, the PCE values of the corresponding devices were very similar (8.52% for Ir-Blue vs. 8.53% for Ir-Red). This was because Ir-Blue exhibits better molecular compatibility with PTB7, resulting in an increase in the crystallinity of the active film.

Table 2.4 Summary of device performances with 5wt%, 10wt% and 15wt% of Ir-Orange.

PTB7_Ir(III) complexes	J_{SC} (mAcm ⁻²)	V_{OC} (V)	FF (%)	PCE (%)
PTB7_Ref.	13.3	0.75	71.7	7.37
PTB7_Ir-Orange 5wt%	15.6	0.72	71.9	8.06
PTB7_Ir-Orange 10wt%	16.1	0.74	72.9	8.72
PTB7_Ir-Orange 15wt%	16.1	0.71	71.0	8.11

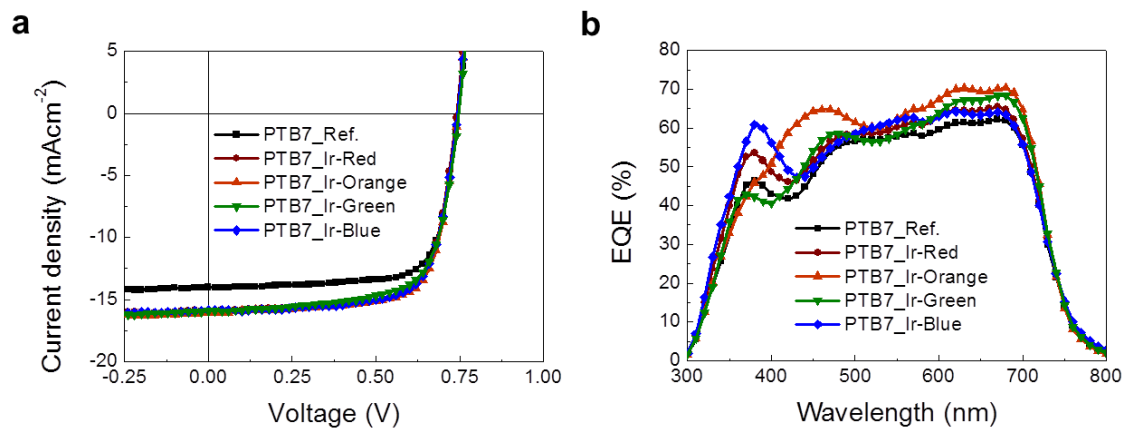


Figure 2.7 (a), J-V curves of the device with 10wt% of various Ir(III) complexes under 1000Wm⁻² and (b), EQE data of devices with 10wt% various Ir(III) complexes

We also fabricated devices with the configuration glass/ITO/ZnO/Ir-Orange/PTB7:PC₇₁BM/MoO₃/Ag, in order to elucidate energy transfer effect in the active layer. Figure 2.9 and Table 2.3 show respectively the J-V curve and the corresponding device results with a separate Ir-Orange complex layer inserted between the ZnO and active layers. The device with the inserted Ir-Orange layer did not exhibit an increase in the J_{SC} (13.3 mAcm⁻² for both). Further, the V_{OC} values were almost similar (0.75 V) and the FF value was slightly lower than that of the reference device (69.9% vs. 71.7%). These results demonstrate that there was no energy transfer in the case of

the inserted Ir-Orange layer, because the FRET radius (<10 nm) was much smaller than the thickness of the active layer (approximately 100 nm). Further, there was no charge transfer from the inserted layer to the active layer. In other words, effective transfer of energy only occurred in the active layer.

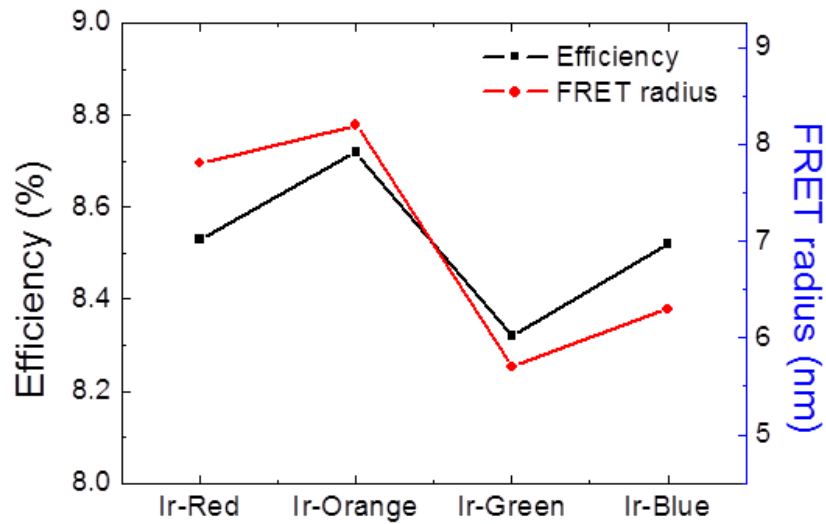


Figure 2.8 Efficiency of devices with Ir(III) complexes (black line) and FRET radius (red line).

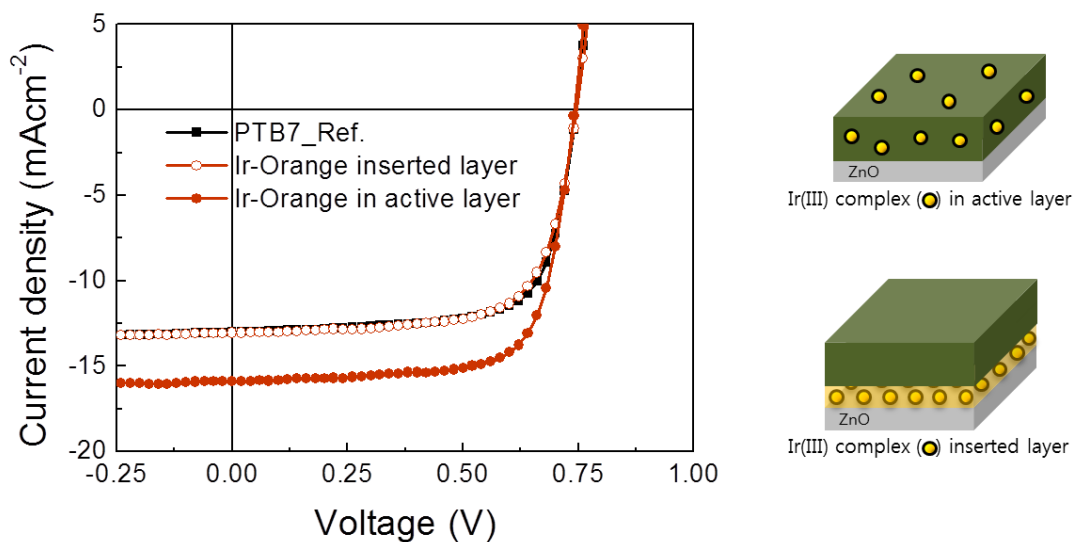


Figure 2.9 Device performances, J - V curves of reference, with Orange inserted layer, and with Orange in active layer.

2.5 Morphological study

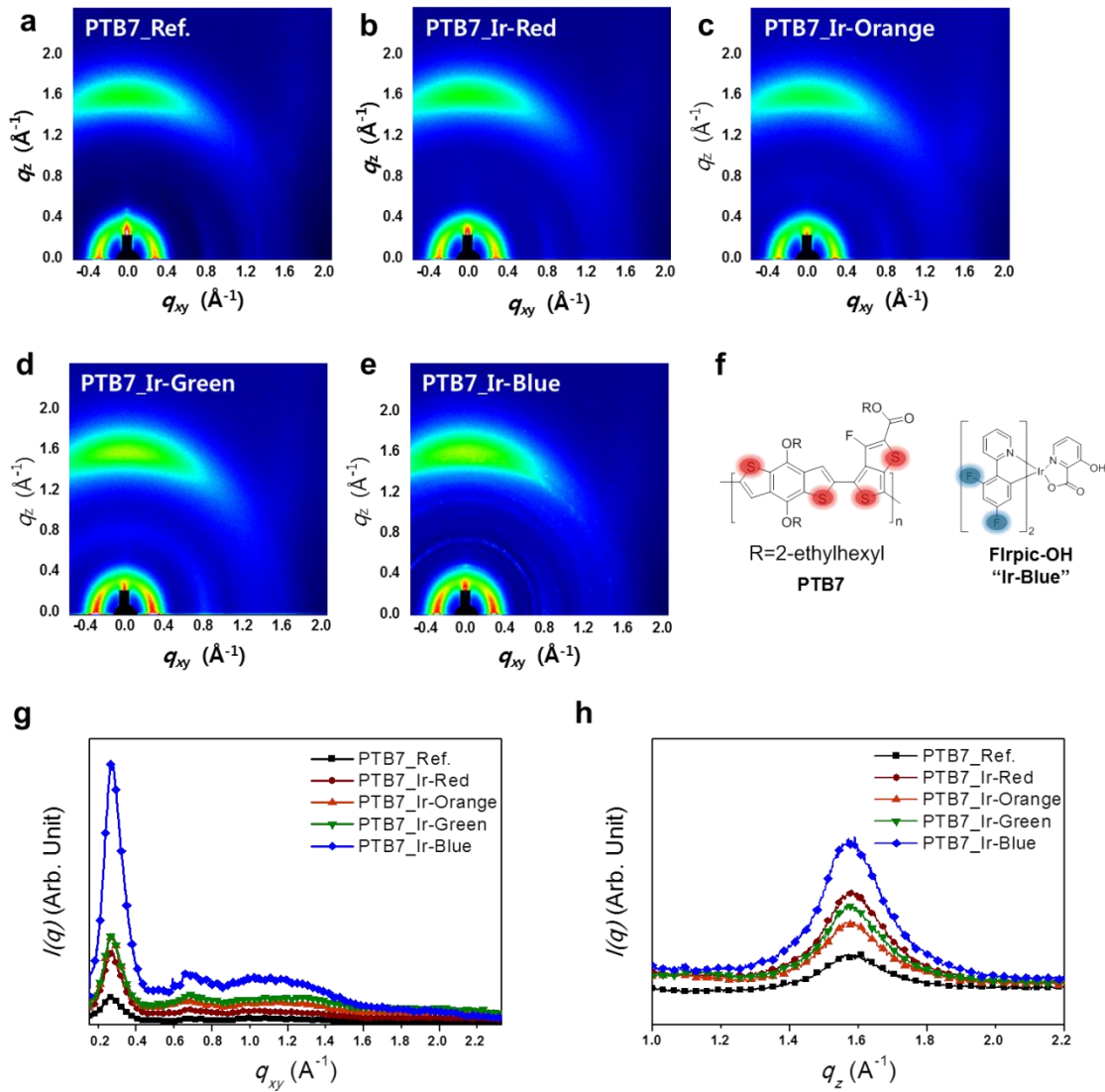


Figure 2.10 2D GI-WAXD patterns of (a) PTB7, (b) PTB7:Ir-Red (10:1), (c) PTB7:Ir-Orange (10:1), (d) PTB7:Ir-Green (10:1), and (e) PTB7:Ir-Blue (10:1). (f) Chemical structures of the incorporated fluorine substituents of Ir-Blue and the thiophene spacers of PTB7. GI-WAXD line-cut profiles of (g) the PTB7:Ir(III) complex system, in-plane. Black square with line: PTB7. Red circle, orange up-triangle, green down-triangle, and blue diamond with line are for Ir-Red, Ir-Orange, Ir-Green, and Ir-Blue with PTB7 respectively. (h) PTB7:Ir(III) complex system, out-of-plane.

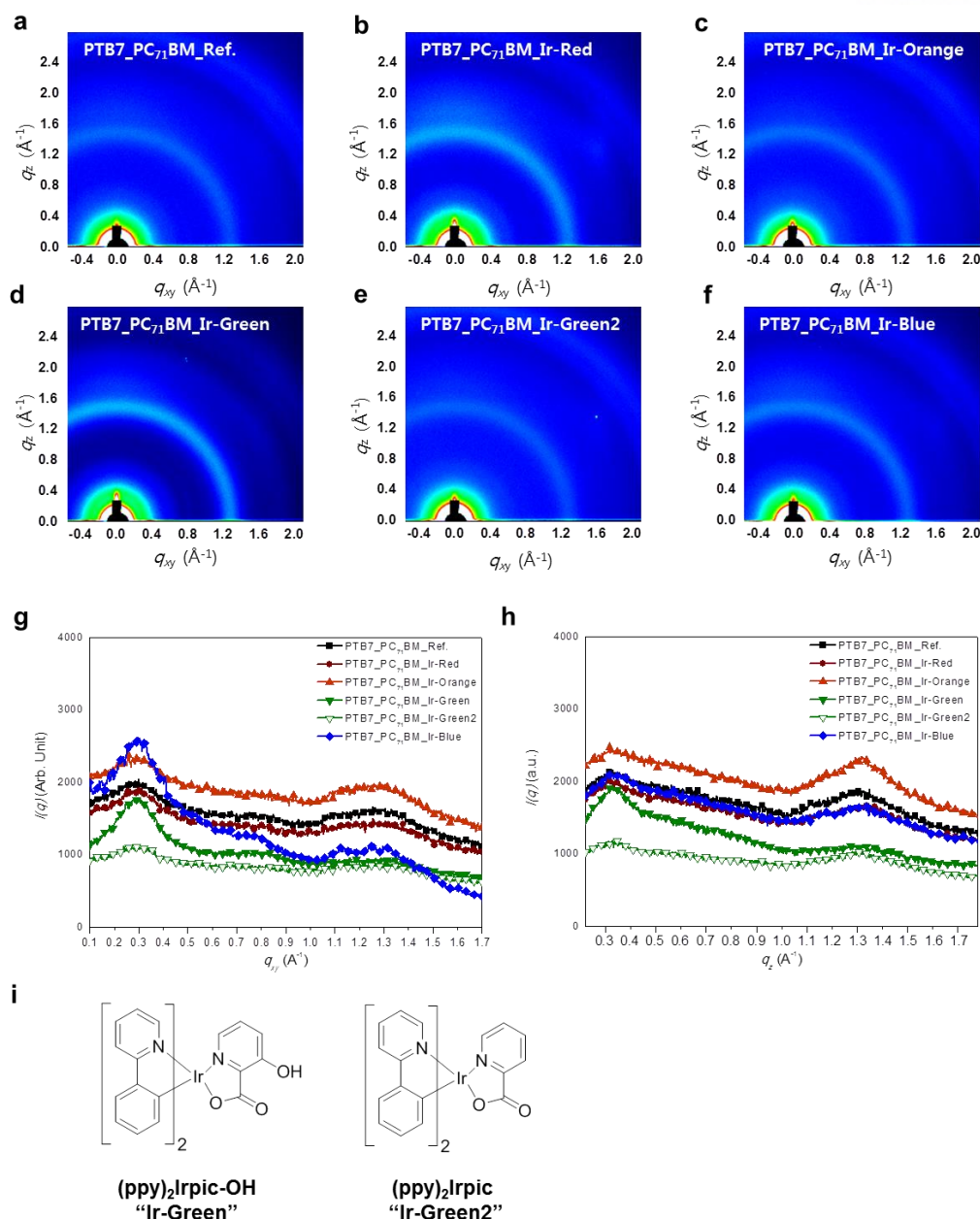


Figure 2.11 2D GI-WAXD patterns and line-cut profiles of PTB7:Ir(III) complex:PC₇₁BM blended films on ZnO modified Si substrate. (a) 2D GI-WAXD patterns of PTB7:PC₇₁BM (1:1.5), (b) PTB7:Ir-Red:PC₇₁BM (1:0.1:1.5), (c) PTB7:Ir-Orange:PC₇₁BM (1:0.1:1.5), (d) PTB7:Ir-Green:PC₇₁BM (1:0.1:1.5), (e) PTB7:Ir-Green2:PC₇₁BM (1:0.1:1.5), (f) PTB7:Ir-Blue:PC₇₁BM (1:0.1:1.5). GI-WAXD line-cut profiles of PTB7:Ir(III) complex:PC₇₁BM system (in-plane, g) and PTB7:Ir(III) complex:PC₇₁BM system (out-of-plane, h). (i) Structure of Ir-Green and Ir-Green2.

The effects of the Ir(III) complexes on the morphology of the energy transfer system layers were investigated using GI-WAXD and AFM. The two-dimensional (2D) GI-WAXD patterns of both the pristine polymer film and the films containing 10 wt% Ir(III) complexes were acquired (Figure 2.10 and 2.11). The (100) diffraction peak at q_{xy} $0.323 \pm 0.007 \text{ \AA}^{-1}$ was observed along the q_{xy} direction (in-plane), while a distinct diffraction peak related to π - π stacking was observed at $q_z = 1.60 \pm 0.05 \text{ \AA}^{-1}$ along the q_z direction (out-of-plane), clearly suggesting a preferential face-on conformation. Further, the Ir(III) complexes did not cause any significant changes in the nanoscale morphology of the PTB7 films.²⁸

Table 2.5 2D GI-WAXD parameters of the PTB7:Ir(III) complex:PC₇₁BM blended systems.

PTB7:Ir(III) complex:PC ₇₁ BM Ratio	q_r (\AA^{-1})	q_r (\AA^{-1})	D_L (\AA)	q_z (\AA^{-1})	q_z (\AA^{-1})	D_L (\AA)
1 : 0 : 0	0.346	0.128	46.1	—	—	—
1 : Ir-Red 10wt% : 0	0.342	0.119	49.6	—	—	—
1 : Ir-Orange 10wt% : 0	0.343	0.110	53.6	—	—	—
1 : Ir-Green 10wt% : 0	0.344	0.122	48.4	—	—	—
1 : Ir-Blue 10wt% : 0	0.345	0.114	51.8	—	—	—
1 : 0 : 1.5	0.356	0.095	62.2	1.37	0.35	16.7
1 : Ir-Red 10wt% : 1.5	0.353	0.089	66.4	1.37	0.34	17.1
1 : Ir-Orange 10wt% : 1.5	0.351	0.089	66.4	1.36	0.32	18.3
1 : Ir-Green 10wt% : 1.5	0.355	0.097	60.9	1.35	0.30	19.5
1 : Ir-Blue 10wt% : 1.5	0.352	0.088	67.1	1.38	0.31	18.8

When the complexes were incorporated into the PTB7:PC₇₁BM blended films (PTB7:10 wt% Ir-Red:PC₇₁BM, PTB7:10 wt% Ir-Orange:PC₇₁BM, PTB7:10 wt% Ir-Green:PC₇₁BM, and PTB7:10 wt% Ir-Blue:PC₇₁BM), they had little effect on the crystal structure of PTB7. The full width at half maximum (FWHM) of the scattering peak, Δq_r , can be correlated to the nanocrystallite size via the Scherrer equation.²⁸⁻³⁰ The Δq values of the peaks of the active layers with the Ir(III) complexes indicate that the incorporation of the Ir(III) complexes into the PTB7:PC₇₁BM blended films resulted in the formation of nanocrystallites (size = D_L) larger than those of the pristine PTB7:PCBM blended film (Table 2.5).^{9,31} In the case of Ir-Orange, D_L of (100) increased from 46.1 Å (PTB7 film) to 51.8 Å (PTB7:Ir-Orange film). It is intriguing that, when PTB7 and the Ir(III) complexes were blended together, the amphiphilic nature of the complexes enhanced the crystallinities of PTB7 and PC₇₁BM, as evidenced by the changes in the GI-WAXD peaks of the periodic layers of PTB7 and Ir(III) complexes and their corresponding FWHMs (Figure 2.11 and Table 2.5). For example, in the case of Ir-Blue, the D_L of the q_r vector was enhanced from 62.2 Å to 67.1 Å, while the D_L of the π - π stacking was enhanced from 16.7 Å to 18.8 Å. Ir-Green exhibited the biggest increase in the D_L of q_z , from 16.7 Å to 19.5 Å, corresponding to about 5 layers of π - π stacking. The enhanced molecular compatibility was related to the 3-hydroxypicolinic acid unit of the Ir(III) complexes. By comparing the GI-WAXD peaks of Ir-Green with those of (ppy)₂Irpic (Ir-Green2, no hydroxyl unit) in PTB7:PC₇₁BM blended films, Ir-Green2 clearly had an adverse effect on the morphologies of PTB7:PC₇₁BM, resulting in weaker GI-WAXD peaks (Figure 2.11). This effect was also confirmed by AFM experiments, showing higher root-mean-square value of Ir-Green2 than that of Ir-Green (see Figure 2.12).

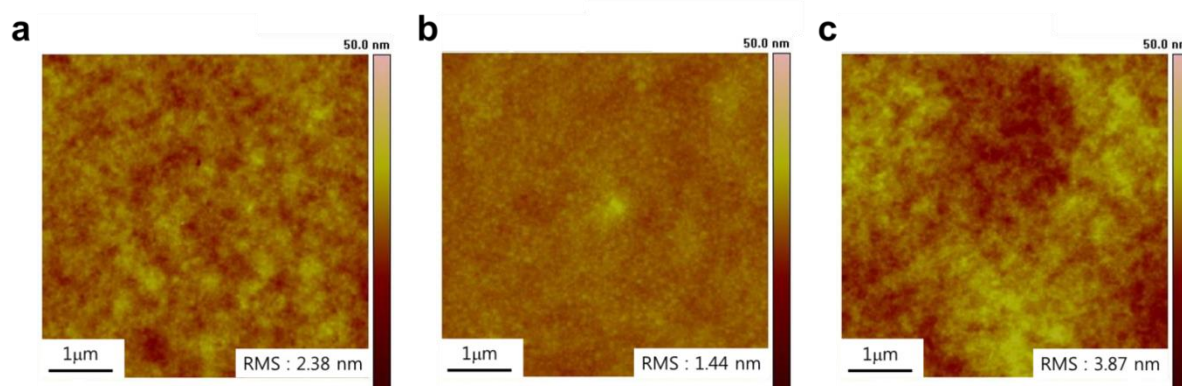


Figure 2.12 (a) 2D AFM image of PTB7:PC₇₁BM blended film, (b) 2D AFM image of PTB7:PC₇₁BM blended film with Ir-Green, (c) 2D AFM image of PTB7:PC₇₁BM blended film with Ir-Green2.

2.6 Compatibility studies of Ir(III) complexes in high-crystallinity polymer P3HT

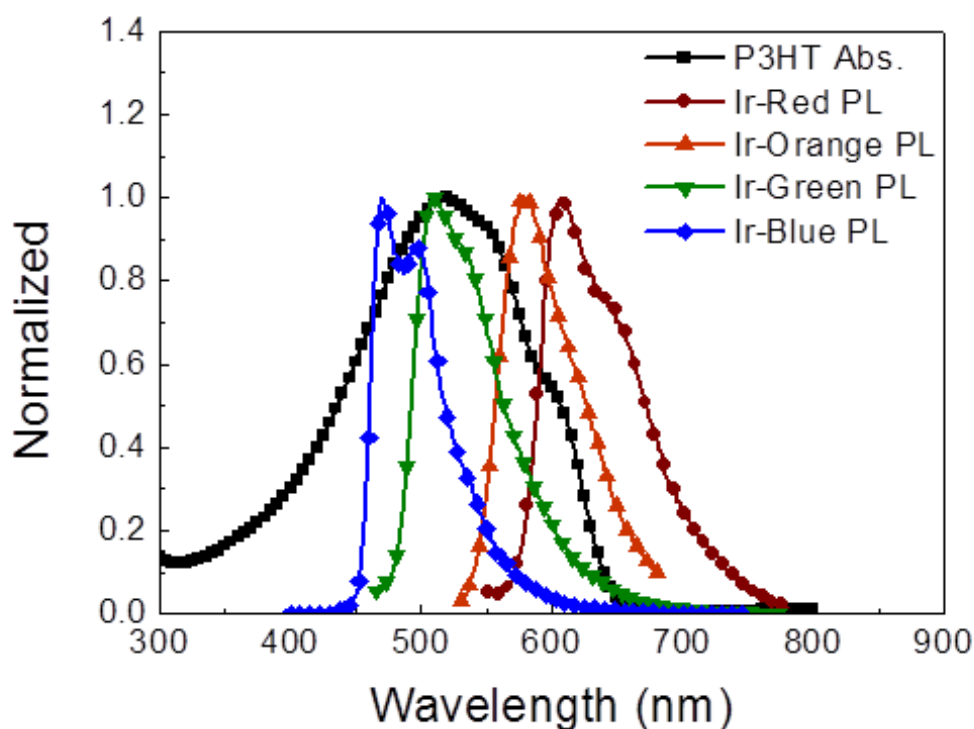


Figure 2.13 Overlap between emission of Ir(III) complexes and absorption of P3HT.

Table 2.6 Optical properties, electrochemical properties, QY values, FRET radii, and device performances for the Ir(III) complexes.

P3HT_Ir(III) complexes	J_{SC} (mAcm ⁻²)	V_{oc} (V)	FF (%)	Best PCE (%)	Average PCE (%)
P3HT_Ref.	10.3	0.57	51.7	3.02	2.96 ± 0.06
P3HT_Ir-Orange	11.0	0.57	51.6	3.23	3.08 ± 0.15
P3HT_Ir-Blue	11.5	0.58	55.9	3.63	3.52 ± 0.11

We also fabricated devices with the Ir(III) complexes as the energy donor, the high-crystallinity polymer P3HT as the energy acceptor and charge donor, and PC₆₁BM as the charge acceptor. The complexes Ir-Blue and Ir-Orange, which have relatively higher FRET radii (Figure 2.13), were selected in order to determine a suitable energy donor for P3HT. The J_{SC} of the P3HT devices based on Ir-Blue and Ir-Orange increased from 10.3 to 11.5 and 11.0 mAcm⁻² respectively, compared to the reference device. They correspond to PCE values of 3.63% for P3HT with Ir-Blue and 3.23% for P3HT with Ir-Orange (Figure 2.14 and Table 2.6). The PCE increased by more than 20% in the case of Ir-Blue, compared to that of the device without an energy donor (PCE 3.02%). This was because Ir-Blue has the largest FRET radius with respect to P3HT, and it also helps in maintaining the crystallinity of P3HT; the latter is supported by the GI-WAXD data (Figure 2.15). To demonstrate the energy transfer from Ir(III) complexes to P3HT, we measured the enhancement of J_{SC} of P3HT cooperated with Ir-Orange using a 463 nm laser (with a power of 200 Wm⁻²), as this wavelength falls in the MLCT region of Ir-Orange. The J_{SC} of Ir-Orange increased from 5.89 to 6.29 mAcm⁻², which is strong evidence for the energy transfer between Ir-Orange and P3HT (Table 2.7).

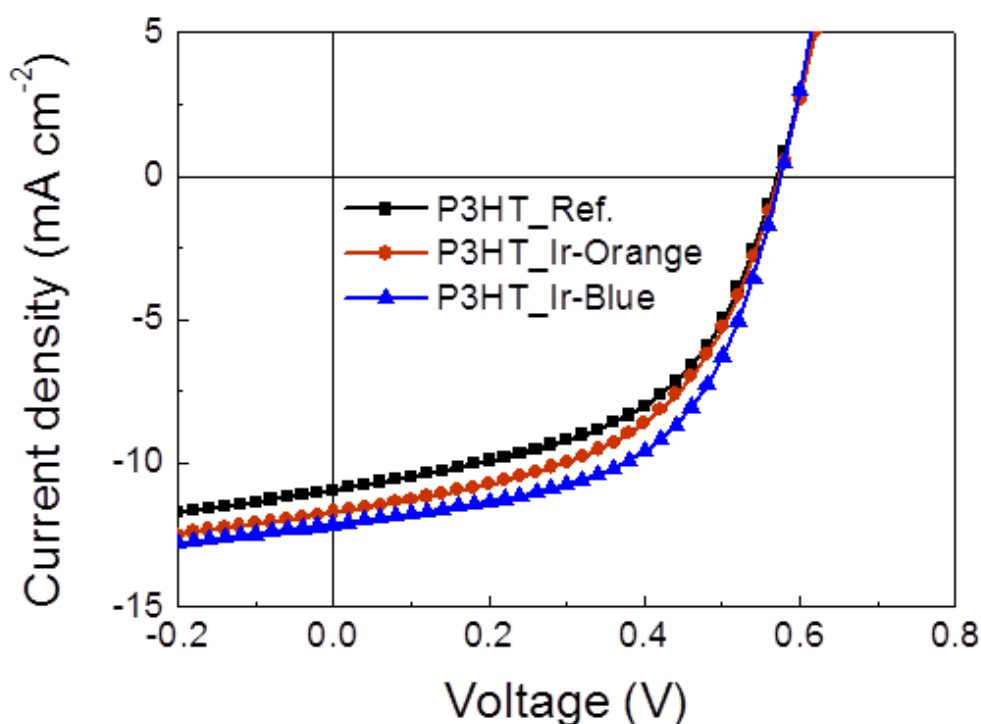


Figure 2.14 Device performance, J-V curves of P3HT reference, Ir-Orange in active layer and Ir-Blue in active layer

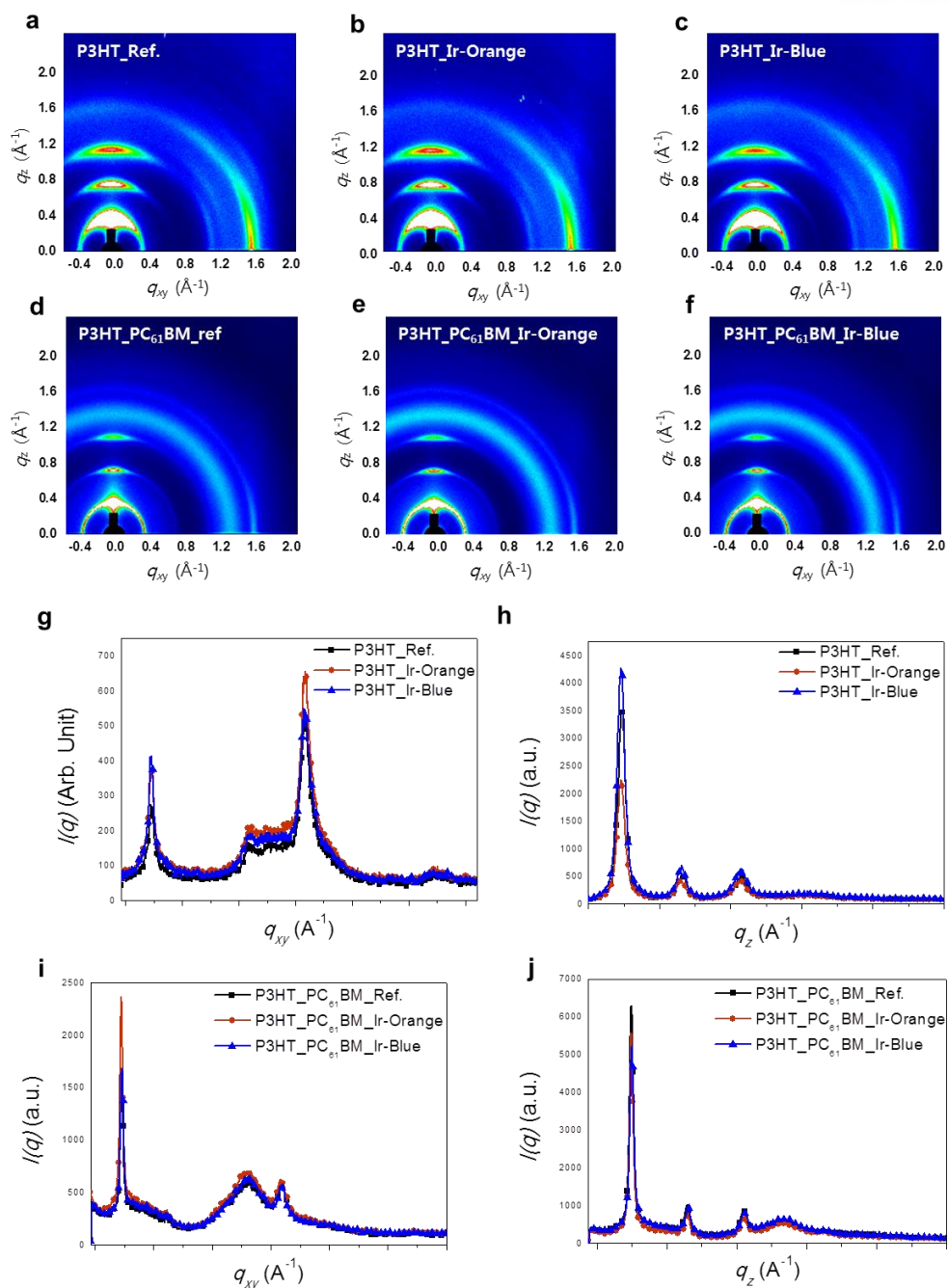


Figure 2.15 (a) 2D GI-WAXD patterns of P3HT, (b) P3HT:Ir-Orange (10:0.05), (c) P3HT:Ir-Blue (10:0.05), (d) P3HT:PC₆₁BM (10:8), (e) P3HT:Ir-Orange:PC₆₁BM (10:0.05:8), (f) P3HT:Ir-Blue:PC₆₁BM (10:0.05:8). GI-WAXD line-cut profiles of P3HT:Ir(III) complexes system (in-plane, g), P3HT:Ir(III) complexes system (out-of-plane, h), P3HT:Ir(III) complexes:PC₆₁BM system (in-plane, i), and P3HT:Ir(III) complexes:PC₆₁BM system (out-of-plane, j).

Table 2.7 Summary of device performances with Orange under 463nm and 200Wm⁻².

P3HT_Ir(III) complexes	J_{SC} (mAcm⁻²)	V_{OC} (V)	FF (%)	PCE (%)
P3HT_Ref.	5.89	0.58	50.2	8.53
P3HT_Ir-Orange 0.5wt%	6.29	0.58	50.4	9.22

2.7 Conclusion

We have successfully demonstrated that the PCEs of PSCs can be increased through energy transfer, by using Ir(III) complexes customized for both amorphous PTB7 and high-crystallinity P3HT active materials. In the case of the PTB7-based devices, PCE could be increased by 18% compared to that of the reference cell when Ir-Orange was used as the energy donor, owing to the dramatic increase (21%) in the J_{SC} by the broadened absorption range of the active layer. To date, the biggest challenge with regard to multicomponent blended PSC system is the optimization of the film morphology. Ir(III) complexes are ideal materials to achieve this goal as they do not affect the morphology of the active layer, because their amphiphilic structure allows them to perform the role of a surfactant at the donor/acceptor interface. As a result, the synthesized Ir(III) complexes are suitable for polymer based PSCs using either the amorphous PTB7 or the high-crystallinity P3HT active materials. In summary, molecular engineered Ir(III) complexes are successfully used as highly customized energy donors for various energy acceptors to improve the performance of PSCs, owing to their tunable energy band gaps and amphiphilic property. This work opens up new design directions for energy transfer systems based on customized energy donor materials to produce high-performance PSCs.

III. Experimental Method and Materials

3.1 Synthesis of Ir(III) complexes

Bis[1-phenylisoquinoline-C2,N](3-hydroxypicolinato)iridium(III)

The mixture of $\text{IrCl}_3 \cdot n\text{H}_2\text{O}$ (200 mg, 0.67 mmol) and 1-phenylisoquinoline (412 mg, 2.00 mmol) was refluxed for 24 h in a 3:1 (v/v) mixture of 2-methoxyethanol and water as solvent. After refluxing the mixture was cooled down to room temperature and more water was added to precipitate the product. The precipitate was filtered through a Büchner funnel and washed with hexane three times to obtain the product (355 mg, 83 % yield).³² A mixture of synthesized product (300 mg, 0.24 mmol), 3-hydroxypicolinic acid (100 mg, 0.72 mmol) and Na_2CO_3 (254 mg, 2.40 mmol) was refluxed for 10–12 h in inert condition in 2-ethoxyethanol as a solvent. After refluxing, the mixture was cooled down to room temperature and the solvent was evaporated. The mixture is dissolved in methylene chloride and then washed with water and dried over MgSO_4 . The solvent was evaporated to obtain the crude product, which was purified by column chromatography on silica gel to afford the final product (238 mg, 367% yield).³³ The characterization data of this product is provided in Figure 3.1, 3.2 and 3.3. Other Ir(III) complexes (2pq)₂Irpic-OH (Orange), (ppy)₂Irpic-OH (Green), and FlIrpic-OH (Blue) were synthesized with similar procedure.

FT-IR (KBr, cm^{-1}): 3440 (w, -OH), 1635 (s, C=O), 1598 (m), 1462 (m), 1380 (w), 1313 (m).

¹H NMR (400 MHz, CDCl_3): δ 13.836 (s, 1H), 8.961 (m, 2H), 8.658 (d, $J=6.4$ Hz, 1H), 8.257 (d, $J=7.6$ Hz, 1H), 8.194 (d, $J=7.6$ Hz, 1H), 7.937 (m, 1H), 7.880 (m, 1H), 7.734 (m, 4H), 7.517 (d, $J=6.8$ Hz, 1H), 7.450 (d, $J=6.4$ Hz, 1H), 7.367 (m, 1H), 7.320 (d, $J=6.4$ Hz, 1H), 7.156 (m, 1H), 7.097 (m, 1H), 7.007 (m, 1H), 6.942 (m, 1H), 6.774 (m, 1H), 6.715 (m, 1H), 6.491 (d, $J=6.8$ Hz, 1H), 6.222 (d, $J=6.8$ Hz, 1H).

¹³C NMR (100 MHz, CDCl_3): δ 177.50, 170.17, 168.23, 160.53, 151.77, 150.40, 146.00, 145.76, 140.71, 140.22, 139.72, 137.06, 137.00, 134.85, 133.05, 131.11, 131.01, 130.16, 130.06, 129.96, 129.61, 128.11, 128.02, 127.56, 127.36, 127.07, 126.47, 126.42, 126.31, 126.17, 121.45, 120.83, 120.81, 120.70.

Exact mass: 739.1447, found mass: 739.1450.

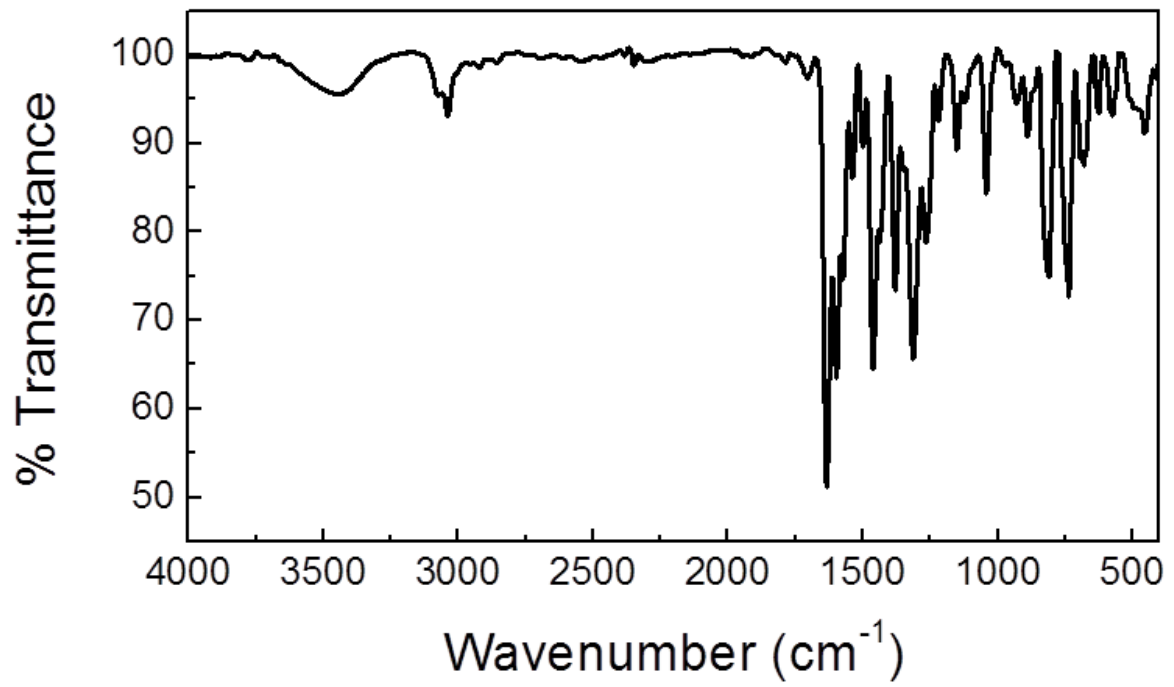


Figure 3.1 IR spectrum of $(1pq)_2Irpic-OH$ (Ir-Red) in KBr pellet.

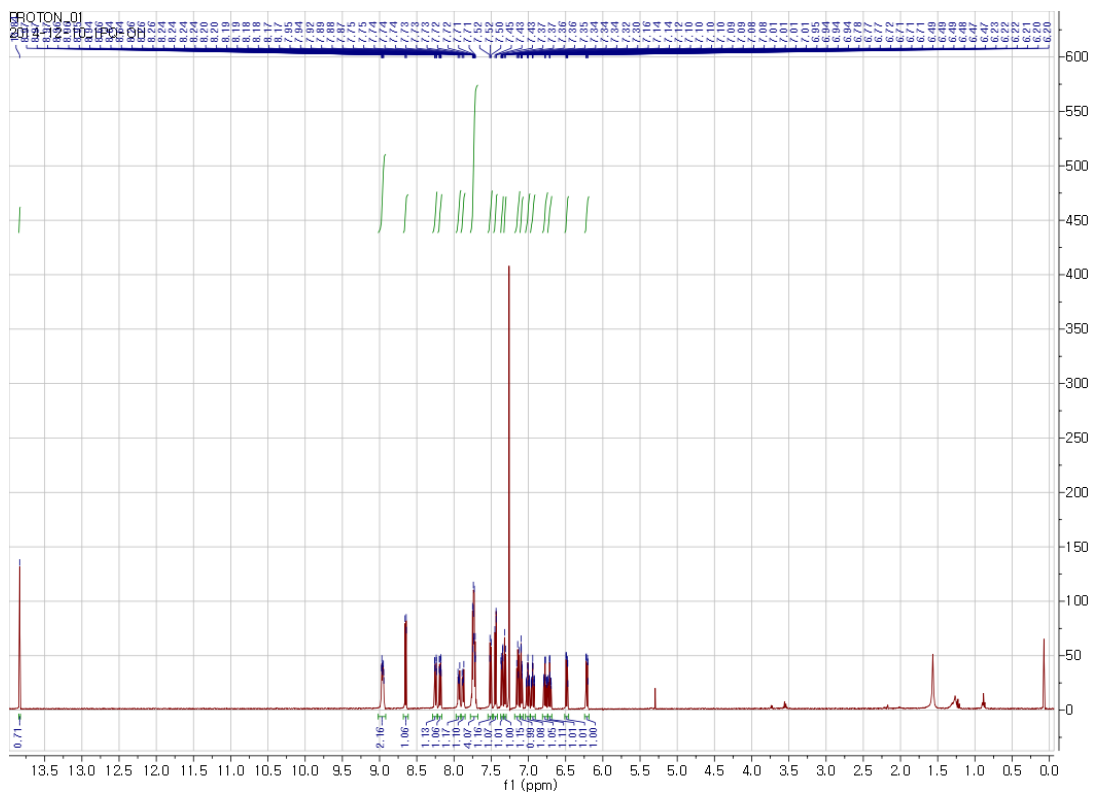


Figure 3.2 1H NMR of $(1pq)_2Irpic-OH$ (Ir-Red) in $CDCl_3$.

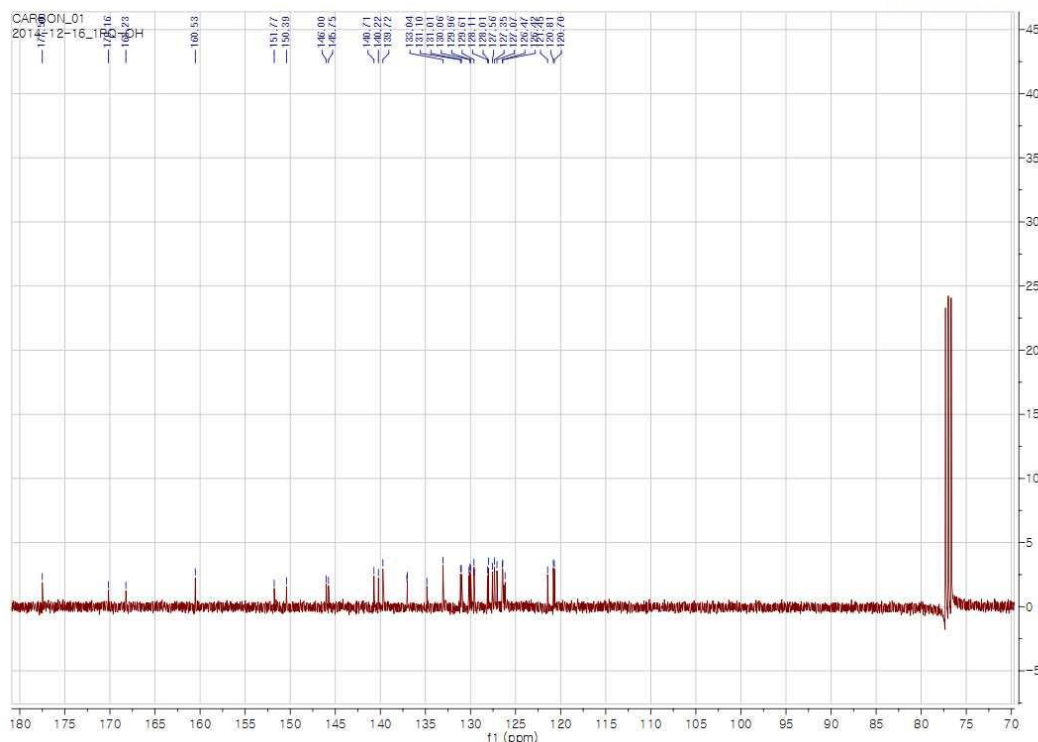


Figure 3.3 ^{13}C NMR of $(1\text{pq})_2\text{Irpic-OH}$ (Ir-Red) in CDCl_3 .

$(2\text{pq})_2\text{Irpic-OH}$ (Ir-Orange)

FT-IR (KBr, cm^{-1}): 3441 (w, -OH), 1636 (s, C=O), 1601 (s), 1461 (s), 1330 (m).

^1H NMR (400 MHz, CDCl_3): δ 13.415 (s, 1H), 8.646 (d, $J=8.8$ Hz, 1H), 8.210 (d, $J=16.8$ Hz, 1H), 8.189 (d, $J=16.8$ Hz, 1H), 8.107 (m, 2H), 7.951 (dd, $J=8$ Hz, 1H), 7.835 (dd, $J=8$ Hz, 1H), 7.741 (m, 2H), 7.554 (m, 1H), 7.475 (m, 2H), 7.358 (m, 2H), 7.12 (m, 2H), 7.099 (m, 1H), 6.987 (m, 1H), 6.953 (m, 1H), 6.862 (m, 1H), 6.775 (m, 1H), 6.666 (m, 1H), 6.286 (dd, $J=6.8$ Hz, 1H).

^{13}C NMR (100 MHz, CDCl_3): δ 176.26, 170.87, 169.11, 159.63, 149.46, 149.17, 148.40, 147.78, 146.72, 145.71, 138.82, 138.65, 137.10, 136.10, 135.78, 134.79, 131.81, 129.94, 129.83, 129.63, 128.81, 128.74, 127.89, 127.80, 127.34, 127.08, 126.74, 126.17, 126.10, 126.03, 125.75, 125.04, 122.18, 121.28, 117.18, 116.43.

Exact mass: 739.1447, found mass: 739.1450.

$(\text{ppy})_2\text{Irpic-OH}$ (Ir-Green)

FT-IR (KBr, cm^{-1}): 3423 (w, -OH), 1632 (s, C=O), 1601 (m), 1471 (s), 1315 (m), 1256 (m), 1249 (m)

^1H NMR (400 MHz, CDCl_3): δ 13.812. (s,1H), 8.717 (m, 1H), 7.894 (d, $J=17.2$ Hz, 1H), 7.874 (d,

$J=16.8$ Hz, 1H), 7.747 (m, 2H), 7.605 (m, 2H), 7.520 (m, 1H), 7.381 (m, 1H), 7.253 (m, 1H), 7.184 (m, 2H), 6.987 (m, 1H), 6.941 (m, 1H), 6.889 (m, 1H), 6.807 (m, 1H), 6.770 (m, 1H), 6.374 (dd, $J=7.6$ Hz, 1H), 6.200 (dd, $J=7.6$ Hz, 1H).

^{13}C NMR (100 MHz, CDCl_3): δ 177.53, 169.14, 167.51, 160.56, 148.81, 148.57, 148.10, 145.94, 144.17, 143.88, 139.70, 137.33, 137.18, 134.84, 132.53, 132.40, 129.95, 129.67, 129.57, 126.44, 124.28, 124.13, 122.29, 122.14, 121.77, 121.17, 119.03, 118.53.

Exact mass: 639.1134, found mass: 639.1136.

(F_2ppy)Irpic-OH (Ir-Blue)

FT-IR (KBr, cm^{-1}): 3432 (w, -OH), 1639 (m, C=O), 1601 (s), 1477 (m), 1404 (m), 1313 (m), 1249 (m).

^1H NMR (400 MHz, CDCl_3): δ 13.569 (s, 1H), 8.674 (m, 1H), 8.314 (m, 1H), 8.257 (d, $J=8.4$ Hz, 1H), 7.821 (m, 2H), 7.480 (m, 1H), 7.446 (m, 1H), 7.263 (m, 2H), 7.243 (m, 1H), 7.047 (m, 1H), 6.505 (m, 1H), 6.440 (m, 1H), 5.793 (m, 1H), 5.586 (m, 1H).

^{13}C NMR (100 MHz, CDCl_3): δ 177.42, 160.68, 148.54, 148.00, 139.56, 138.42, 138.31, 134.30, 129.97, 127.26, 123.42, 123.23, 122.91, 122.72, 122.61, 122.47, 114.60, 114.57, 114.42, 114.39, 98.61, 98.34, 98.12, 97.85, 97.59.

Exact mass: 711.0757, found mass: 711.0755.

3.2 Fabrication of inverted PSCs

3.2.1 Device with PTB7

The ITO-coated glass substrate was cleaned using a substrate-cleaning disinfectant by ultrasonication in deionized (DI) water, acetone, and isopropyl alcohol, respectively, on a heating hotplate, and finally treated in a UV-ozone chamber for 20 min.

To obtain an amorphous-ZnO layer for use in the spin-coating method, 1.64 g of zinc acetate (Aldrich) was first dissolved in 10 g of 2-methoxyethanol, to which 0.5 g of ethanol amines was added to confirm complete dissolution of the zinc acetate. Then, 8 mg of PTB7, 12 mg of PC_{71}BM (1-Material Chemscitech) and 0.8 mg of synthesized Ir(III) complex compound were dissolved in 0.97 ml of chlorobenzene to perform as an electron donor (PTB7) and electron acceptor (PC_{71}BM) material. This bulk-heterojunction material was mixed with 0.03 ml of 1,8-diiodooctane (Sigma Aldrich) and stirred for 12 h at 60°C in a nitrogen glove box. The active solutions were filtered using a $0.2\ \mu\text{m}$ polytetrafluoroethylene syringe filter. To create the cathodes for the Inverted PSCs, an ITO-coated glass substrate was cleaned with oxygen plasma, and then spin-coated with a liquid ZnO sol-gel for 30

s at a speed of 3000 rpm. The ZnO layer formed on the glass substrate was annealed for 10 min at 200°C in air. Next, to create the active layer, the bulk-heterojunction material was spin-coated on top of the ZnO layer at the spin speed of 1200 rpm for 60 s. The device fabrication was completed by thermal evaporation of 4 nm MoO₃ and 70 nm Ag using a shadow mask as the anode under vacuum at a base pressure of 3×10^{-6} Torr. The anode area in the final device was 0.138 cm².

3.2.2 Device with P3HT

To obtain active layer for use in the spin-coating method, 25.8 mg of P3HT, 20.5 mg of PC₆₁BM (1-Material Chemscitech) and 0.13 mg of synthesized Ir(III) complex compound were dissolved in 1 ml dichlorobenzene to perform as an electron donor (P3HT) and electron acceptor (PC₆₁BM) material. This bulk-heterojunction material was mixed and stirred for 12 h at 60°C in a nitrogen glove box. The active solutions were filtered using a 0.2 μm polytetrafluoroethylene syringe filter. To create the cathodes for the Inverted PSCs, an ITO-coated glass substrate was cleaned with oxygen plasma, and then spin-coated with poly(3,4-ethylenedioxythiophene) polystyrene sulfonate (PEDOT:PSS) for 45 s at a speed of 4000 rpm. The PEDOT:PSS layer formed on the ITO-coated glass substrate was annealed for 10 min at 140°C in air. Next, to make an active layer, the bulk-heterojunction material was spin-coated on top of ZnO layer at the spin speed of 600 rpm for 60 s. The device fabrication was completed by thermal evaporation of 100 nm Al using a shadow mask as the anode under vacuum at a base pressure of 3×10^{-6} Torr. The anode area in the final device was 0.138 cm².

The device was measured in a glovebox with nitrogen atmosphere by recording the *J-V* curves with a Keithley 2635 A under simulated AM1.5G radiation (1000 Wm⁻²) using a xenon arc lamp.

3.3 Morphological study

Atomic force microscopy (AFM) images were obtained using a Veeco microscope in tapping mode over a 1 mm² scan area. 2D GI-WAXD measurements were carried out at PLS-II 6D UNIST-PAL beamline of Pohang Accelerator Laboratory in Korea. The X-rays coming from the bending magnet are monochromated ($\lambda = 1.06 \text{ \AA}$) using a double crystal monochromator (DCM) and are focused using a sagittal focusing DCM and bendable toroidal mirror system (beam size: 150 (H) x 120 (V) μm² in FWHM @ sample position). 2D GI-WAXD measurement system is equipped with a 6-axis motorized sample stage inside a vacuum chamber ($\sim 2 \times 10^{-2}$ Torr), thus the fine alignment of a thin film sample and effective removing of unwanted air and window scattering is possible. 2D GI-WAXD patterns were recorded with a 2D CCD detector (Rayonix MX225-HS, USA) and diffraction angles were calibrated by a pre-calibrated sucrose (Monoclinic, P21, $a = 10.8631 \text{ \AA}$, $b = 8.7044 \text{ \AA}$, $c = 7.7624 \text{ \AA}$, $\beta = 102.938^\circ$).

References

- (1) Yu, G.; Gao, J.; Hummelen, J. C.; Wudl, F.; Heeger, A. J. Polymer Photovoltaic Cells: Enhanced Efficiencies Via a Network of Internal Donor-Acceptor Heterojunctions. *Science* **1995**, *270*, 1789-1791.
- (2) Schilinsky, P.; Waldauf, C.; Brabec, C. J. Recombination and Loss Analysis in Polythiophene Based Bulk Heterojunction Photodetectors. *Appl. Phys. Lett.* **2002**, *81*, 3885-3887.
- (3) He, Y.; Zhao, G.; Peng, B.; Li, Y. High-Yield Synthesis and Electrochemical and Photovoltaic Properties of Indene-C70 Bisadduct. *Adv. Funct. Mater.* **2010**, *20*, 3383-3389.
- (4) Liang, Y.; Xu, Z.; Xia, J.; Tsai, S.-T.; Wu, Y.; Li, G.; Ray, C.; Yu, L. For the Bright Future—Bulk Heterojunction Polymer Solar Cells with Power Conversion Efficiency of 7.4%. *Adv. Mater.* **2010**, *22*, E135-E138.
- (5) He, Z.; Xiao, B.; Liu, F.; Wu, H.; Yang, Y.; Xiao, S.; Wang, C.; Russell, T. P.; Cao, Y. Single-Junction Polymer Solar Cells with High Efficiency and Photovoltage. *Nat. Photon.* **2015**, *9*, 174-179.
- (6) Liu, Y.; Zhao, J.; Li, Z.; Mu, C.; Ma, W.; Hu, H.; Jiang, K.; Lin, H.; Ade, H.; Yan, H. Aggregation and Morphology Control Enables Multiple Cases of High-Efficiency Polymer Solar Cells. *Nat. Commun.* **2014**, *5*, 5293.
- (7) Koppe, M.; Egelhaaf, H.-J.; Dennler, G.; Scharber, M. C.; Brabec, C. J.; Schilinsky, P.; Hoth, C. N. Near Ir Sensitization of Organic Bulk Heterojunction Solar Cells: Towards Optimization of the Spectral Response of Organic Solar Cells. *Adv. Funct. Mater.* **2010**, *20*, 338-346.
- (8) Lu, L.; Zheng, T.; Wu, Q.; Schneider, A. M.; Zhao, D.; Yu, L. Recent Advances in Bulk Heterojunction Polymer Solar Cells. *Chem. Rev.* **2015**, *115*, 12666-12731.
- (9) Lu, L.; Xu, T.; Chen, W.; Landry, E. S.; Yu, L. Ternary Blend Polymer Solar Cells with Enhanced Power Conversion Efficiency. *Nat. Photon.* **2014**, *8*, 716-722.
- (10) Yang, Y.; Chen, W.; Dou, L.; Chang, W.-H.; Duan, H.-S.; Bob, B.; Li, G.; Yang, Y. High-Performance Multiple-Donor Bulk Heterojunction Solar Cells. *Nat. Photon.* **2015**, *9*, 190-198.
- (11) Zhang, S.; Zuo, L.; Chen, J.; Zhang, Z.; Mai, J.; Lau, T.-K.; Lu, X.; Shi, M.; Chen, H. Improved Photon-to-Electron Response of Ternary Blend Organic Solar Cells with a Low Band Gap Polymer Sensitizer and Interfacial Modification. *J. Mater. Chem. A* **2016**, *4*, 1702-1707.
- (12) Gao, L.; Zhang, Z.-G.; Xue, L.; Min, J.; Zhang, J.; Wei, Z.; Li, Y. All-Polymer Solar Cells Based on Absorption-Complementary Polymer Donor and Acceptor with High Power Conversion Efficiency of 8.27%. *Adv. Mater.* **2016**, *28*, 1884-1890.
- (13) Bin, H.; Zhang, Z.-G.; Gao, L.; Chen, S.; Zhong, L.; Xue, L.; Yang, C.; Li, Y. Non-Fullerene

Polymer Solar Cells Based on Alkylthio and Fluorine Substituted 2d-Conjugated Polymers Reach 9.5% Efficiency. *J. Am. Chem. Soc.* **2016**, *138*, 4657-4664.

(14) Zhao, W.; Qian, D.; Zhang, S.; Li, S.; Inganäs, O.; Gao, F.; Hou, J. Fullerene-Free Polymer Solar Cells with over 11% Efficiency and Excellent Thermal Stability. *Adv. Mater.* **2016**, DOI: 10.1002/adma.201600281.

(15) Huang, J.-S.; Goh, T.; Li, X.; Sfeir, M. Y.; Bielinski, E. A.; Tomasulo, S.; Lee, M. L.; Hazari, N.; Taylor, A. D. Polymer Bulk Heterojunction Solar Cells Employing Förster Resonance Energy Transfer. *Nat. Photon.* **2013**, *7*, 479-485.

(16) Lu, L.; Chen, W.; Xu, T.; Yu, L. High-Performance Ternary Blend Polymer Solar Cells Involving Both Energy Transfer and Hole Relay Processes. *Nat. Commun.* **2015**, *6*, 7327.

(17) Gupta, V.; Bharti, V.; Kumar, M.; Chand, S.; Heeger, A. J. Polymer–Polymer Förster Resonance Energy Transfer Significantly Boosts the Power Conversion Efficiency of Bulk-Heterojunction Solar Cells. *Adv. Mater.* **2015**, *27*, 4398-4404.

(18) Lee, W.; Kwon, T.-H.; Kwon, J.; Kim, J.-y.; Lee, C.; Hong, J.-I. Effect of Main Ligands on Organic Photovoltaic Performance of Ir(III) Complexes. *New J. Chem.* **2011**, *35*, 2557-2563.

(19) Yook, K. S.; Lee, J. Y. Solution Processed Multilayer Deep Blue and White Phosphorescent Organic Light-Emitting Diodes Using an Alcohol Soluble Bipolar Host and Phosphorescent Dopant Materials. *J. Mater. Chem.* **2012**, *22*, 14546-14550.

(20) Xu, M.; Zhou, R.; Wang, G.; Xiao, Q.; Du, W.; Che, G. Synthesis and Characterization of Phosphorescent Iridium Complexes Containing Trifluoromethyl-Substituted Phenyl Pyridine Based Ligands. *Inorg. Chim. Acta* **2008**, *361*, 2407-2412.

(21) Adachi, C.; Kwong, R. C.; Djurovich, P.; Adamovich, V.; Baldo, M. A.; Thompson, M. E.; Forrest, S. R. Endothermic Energy Transfer: A Mechanism for Generating Very Efficient High-Energy Phosphorescent Emission in Organic Materials. *Appl. Phys. Lett.* **2001**, *79*, 2082-2084.

(22) Yun, M. H.; Lee, E.; Lee, W.; Choi, H.; Lee, B. R.; Song, M. H.; Hong, J.-I.; Kwon, T.-H.; Kim, J. Y. Enhanced Performance of Polymer Bulk Heterojunction Solar Cells Employing Multifunctional Iridium Complexes. *J. Mater. Chem. C* **2014**, *2*, 10195-10200.

(23) Zhang, D.; Wen, Y.; Xiao, Y.; Yu, G.; Liu, Y.; Qian, X. Bulky 4-Tritylphenylethynyl Substituted Boradiazaindacene: Pure Red Emission, Relatively Large Stokes Shift and Inhibition of Self-Quenching. *Chem. Commun.* **2008**, 4777-4779.

(24) Kwon, T.-H.; Kim, M. K.; Kwon, J.; Shin, D.-Y.; Park, S. J.; Lee, C.-L.; Kim, J.-J.; Hong, J.-I. Highly Efficient Light-Harvesting System Based on a Phosphorescent Acceptor Coupled with Dendrimer Donors Via Singlet–Singlet and Triplet–Triplet Energy Transfer. *Chem. Mater.* **2007**, *19*, 3673-3680.

(25) Wang, J.; Chepelianskii, A.; Gao, F.; Greenham, N. C. Control of Exciton Spin Statistics

- through Spin Polarization in Organic Optoelectronic Devices. *Nat. Commun.* **2012**, *3*, 1191.
- (26) Qian, M.; Zhang, R.; Hao, J.; Zhang, W.; Zhang, Q.; Wang, J.; Tao, Y.; Chen, S.; Fang, J.; Huang, W. Dramatic Enhancement of Power Conversion Efficiency in Polymer Solar Cells by Conjugating Very Low Ratio of Triplet Iridium Complexes to Ptb7. *Adv. Mater.* **2015**, *27*, 3546-3552.
- (27) Hardin, B. E.; Hoke, E. T.; Armstrong, P. B.; Yum, J.-H.; Comte, P.; Torres, T.; Frechet, J. M. J.; Nazeeruddin, M. K.; Gratzel, M.; McGehee, M. D. Increased Light Harvesting in Dye-Sensitized Solar Cells with Energy Relay Dyes. *Nat. Photon.* **2009**, *3*, 406-411.
- (28) Chen, W.; Nikiforov, M. P.; Darling, S. B. Morphology Characterization in Organic and Hybrid Solar Cells. *Energy Environ. Sci.* **2012**, *5*, 8045-8074.
- (29) Smilgies, D.-M. Scherrer Grain-Size Analysis Adapted to Grazing-Incidence Scattering with Area Detectors. *J. Appl. Crystallogr.* **2009**, *42*, 1030-1034.
- (30) Chen, W.; Xu, T.; He, F.; Wang, W.; Wang, C.; Strzalka, J.; Liu, Y.; Wen, J.; Miller, D. J.; Chen, J.; Hong, K.; Yu, L.; Darling, S. B. Hierarchical Nanomorphologies Promote Exciton Dissociation in Polymer/Fullerene Bulk Heterojunction Solar Cells. *Nano Lett.* **2011**, *11*, 3707-3713.
- (31) Lu, X.; Hlaing, H.; Germack, D. S.; Peet, J.; Jo, W. H.; Andrienko, D.; Kremer, K.; Ocko, B. M. Bilayer Order in a Polycarbazole-Conjugated Polymer. *Nat. Commun.* **2012**, *3*, 795.
- (32) Nonoyama, M. Benzo[*H*]Quinolin-10-*Yl-N* Iridium(III) Complexes. *Bull. Chem. Soc. Jpn.* **1974**, *47*, 767-768.
- (33) Kwon, T.-H.; Oh, Y. H.; Shin, I.-S.; Hong, J.-I. New Approach toward Fast Response Light-Emitting Electrochemical Cells Based on Neutral Iridium Complexes Via Cation Transport. *Adv. Funct. Mater.* **2009**, *19*, 711-717.

Acknowledgement

우선 4학년 여름방학부터 3년간 저를 지도해 주신 교수님께 감사의 말씀을 드립니다. 연구에 대해서 전혀 모르고 있을 때 많은 것을 가르쳐 주셨습니다. 덕분에 석사과정 동안 논문을 마무리 할 수 있었습니다. 그리고 제가 길을 찾지 못할 때도 나침반처럼 제가 가야 하는 방향을 찾는데 도움을 주셨습니다. 항상 학생을 생각하시는 진짜 교육자이신 권태혁 교수님께 감사의 말씀을 드립니다.

또한 공동연구를 지도해주신 서관용교수님께도 감사의 말씀을 드립니다. 같이 실험한 현탁이형, 지훈이형에게도 고맙다는 말을 전하고 백명진박사님과 소정, 민수, 은혜에게도 고맙다는 말을 전하고 싶습니다. 다른 일들도 바쁘지만 책임감을 갖고 같이 일했던 현탁이형 고마워요. 제가 OPV 시작할 때 옆에서 봐주고 가르쳐준 지훈이형도 고맙습니다. 합성을 배우면서 많은 도움을 주신 박사님도 저를 보면서 많이 답답하셨을 텐데 정말 고맙습니다. GI-WAXD 찍으면서 친해진 소정님도 연구에 도움이 돼서 고맙게 생각해. 형들이 잡일을 시키고 구박해도 흔들림이 없는 민수도, 많은 도움은 주지 못했지만 같이 합성을 하던 은혜도 고맙다.

이 외에도 3년간 가족처럼 지낸 E. R. Lab 멤버, 전 방장 현규형, 현 방장 정수형, 병만이형, 동향사람 현오형, 광민, 정승, 덕호, 언영, 준혁 그리고 학부생들 역시 실험실 멤버로서 없어서는 안될 중요한 역할을 해주었습니다. 실험실이 흐트러지지 않고 똑바로 서있을 수 있었던 것은 정수형과 현규형의 노력이 있었기에 가능했습니다. 항상 말 잘 듣는 후배는 아니었지만 저를 버리지 않고 데려가 주셔서 감사합니다. 연구분야는 다르지만 옆자리에서 저를 지켜 보면서 조언을 준 병만이형, 싱가포르에서 해주신 말씀 잊지 않고 있습니다. 덕분에 결심을 내릴 수 있었습니다. 고맙습니다. 실험실에서 항상 존재감을 내뿜는 현오형. 저랑 실없는 소리 하면서 놀아줘서 고마워요. 같은 청주에

살지만 청주에서는 본적이 없네요. 언제 한번 청주에서 만나요. 광민, 처음 들어왔을 때 내 옆자리였는데 그때 엄청 어색했던 기억이 나네. 하는 일이 달라서인지 많이 마주칠 기회는 없었지만 지금은 어색하지 않으니 다행이야. 정승이랑 덕호, 준혁이는 알아서 잘 하는 후배들이라 보기 좋았어. 앞으로도 당연히 잘 하겠지? 마지막으로 홍일점 대학원생 언영이는 혼자 여학생이지만 열심히 하는 모습이 멋있다고 생각해. 다른 여 후배들이 들어오면 언니로서 잘 이끌어 갈 거라 믿어.

마지막으로 실험실 밖에서, 항상 제 뒤에서 응원해주신 아버지, 어머니 그리고 누나가 있었기에 석사과정을 마칠 수 있었습니다. 제 주위의 모든 분들께 감사 드립니다.

